plasmid pHelper (Stratagene, La Jolla, CA, USA) into HEK293T cells by calcium phosphate coprecipitation. A large-scale cell culture method with an active gassing system was used for transfection [20]. Cell suspensions were collected 72 h after transfection and centrifuged at 300 *g* for 10 min. Cell pellets were resuspended in 30 ml of Tris-buffered saline [100 mM Tris-HCl (pH 8.0), 150 mM NaCl]. AAV2/8-cMD1 virus was harvested by five cycles of freeze-thawing of the resuspended pellet. The crude viral lysate was initially concentrated by a brief two-tier CsCl gradient centrifugation for 3 h and further purified by dual ion-exchange chromatography [21]. For viral capsid lysis, the same volume of the AL buffer (Qiagen, Hilden, Germany) was added to DNase I-treated viruses and incubated for 10 min at 56 °C. The final number of AAV2/8-cMD1 virus particles was determined by quantitative-polymerase chain reaction (Q-PCR) of DNase I-treated stocks with plasmid standards. Q-PCR was performed using SYBR-green detection of PCR products in real time with the MyiQ single-colour detection system (Bio-Rad, Hercules, CA, USA). Specific primer sets were as follows (5′ to 3′); for canine specific mRNA sequence-optimized microdystrophin, AGGCAGAGCACCAGAAACTACC (forward) and CTGGTACTTGGCGATGTTGAAG (reverse).

Intramuscular administration of AAV

Our experimental dog was a beagle-based *CXMDj* from the breeding colony at National Center of Neurology and Psychiatry (NCNP; Tokyo, Japan). The animal was cared and treated in accordance with the guidelines approved by Ethics Committee for Treatment of Laboratory Animals at NCNP. The *CXMDj* dog (9 weeks of age; $n = 1$) was sedated with isoflurane by mask inhalation and intubated. Anesthesia was maintained with 2–4% isoflurane and *tibialis cranialis* (TC), *extensor carpi radialis* (ECR) and *gastrocnemius* (GC) muscles of the *CXMDj* dog were injected intramuscularly with 1 ml (ECR and TC; left; 1×10^{13} vector genomes TC; right; 1×10^{12} vector genome) and 2 ml (GC; left; 2×10^{13} vector genomes right; saline only) of AAV2/8-cMD1 under ultrasonographic guidance. Four weeks after injection of the viruses, ECR muscle was biopsied and sampled by five-blocks segmentation. The dog was culled 8 weeks after injection and TC, GC muscles and other organs were divided into seven to nine blocks after tendon-to-tendon excisions of the muscles and rapidly frozen in liquid nitrogen-cooled isopentane.

Histological analysis

To assess muscle pathology, 10-μm cryosections of muscles were prepared and dried for 10 min at room temperature and fixed in cold acetone at −20 °C. A number of slides were stained with hematoxylin and eosin (H&E). Slides were immersed in hematoxylin for 5 min, rinsed under running tap water for 5 min, immersed in eosin for 2 min and rinsed for another 5 min. Dehydration in progressively higher concentrated solutions of ethanol (up to 100%) was performed, followed by a final dip in Xylene. H&E stained slides were mounted in DPX mountant. The central nucleated fibers were counted under × 400 magnification in four random areas of H&E stained tissues. The percentage of central nucleation was calculated by dividing the number of central nucleated fibers by total fibers in four random areas of TC muscles. Fixed frozen sections were blocked in 5% goat serum in phosphate-buffered saline containing 0.05% Tween 20 and incubated at room temperature for 1 h. Mouse monoclonal anti-dystrophin antibodies (dilution 1:100; NCL-dysB, Novocastra, Newcastle upon Tyne, UK) were used to detect the N-terminus of the dystrophin molecule. Mouse monoclonal antibodies against α-dystrobrevin (dilution 1:200; BD Biosciences, San Diego, CA, USA) and rabbit polyclonal α1-syntrophin (dilution 1:200; Abcam, Cambridge, MA, USA) were used. The signal was visualized using Alexafluor 568-conjugated anti-mouse immunoglobulin (Ig)G secondary antibodies or Alexafluor 568-conjugated anti-rabbit IgG secondary antibodies (dilution 1:1000; Invitrogen, Carlsbad, CA, USA). Tissues were double-stained with mouse anti-canine CD8α (dilution 1:20; CA9. JD3, Serotec, Kidlington, UK) and rabbit laminin (dilution 1:100; Abcam, Cambridge, MA, USA) antibodies. Signal was amplified using Alexafluor 488-conjugated anti-mouse IgG secondary antibodies (dilution 1:1000; Invitrogen) or Alexafluor 568-conjugated anti-rabbit IgG secondary antibodies (dilution 1:1000; Invitrogen). To examine the level of the sarcolemmal permeability, endogenous intracellular IgG was evaluated in muscle fibers by direct staining using an Alexafluor 488-conjugated sheep anti-canine IgG (dilution 1:200; Serotec).

Detection of microdystrophin viral DNA in muscle tissues

Approximately 20 mg of cryosections of the tissue were prepared and homogenized. Genomic DNA was extracted using a Nucleospin Tissue kit (Macherey-Nagel, Düren, Germany). Levels of genomic DNA were examined by quantitative PCR using SYBR-green detection of PCR products in real time with the MyiQ single-colour detection system (Bio-Rad). Genomic DNA (100 ng) was used in a final volume of 20 μl containing 2 × TakaRa SYBR Ex Tag mix and RNase-free DNase-free water. Specific primers for cMD1 detection were (5′ to 3′): CCAACAAAGTGCCCTACTACATC (forward) and GGTTGTGCTGGTCCAGGGCGT (Reverse). Ultra conserved regions (UCR) [22], which are noncoding genomic regions and conserved between human, dog and mouse, were used as a control for genomic DNA using primers (5′ to 3′): GAACACGCGTTAATAAGGCAATCA (forward) and CTGACATTCATCGCATCTTTGACA (reverse). Reactions were run by denaturation (95 °C for

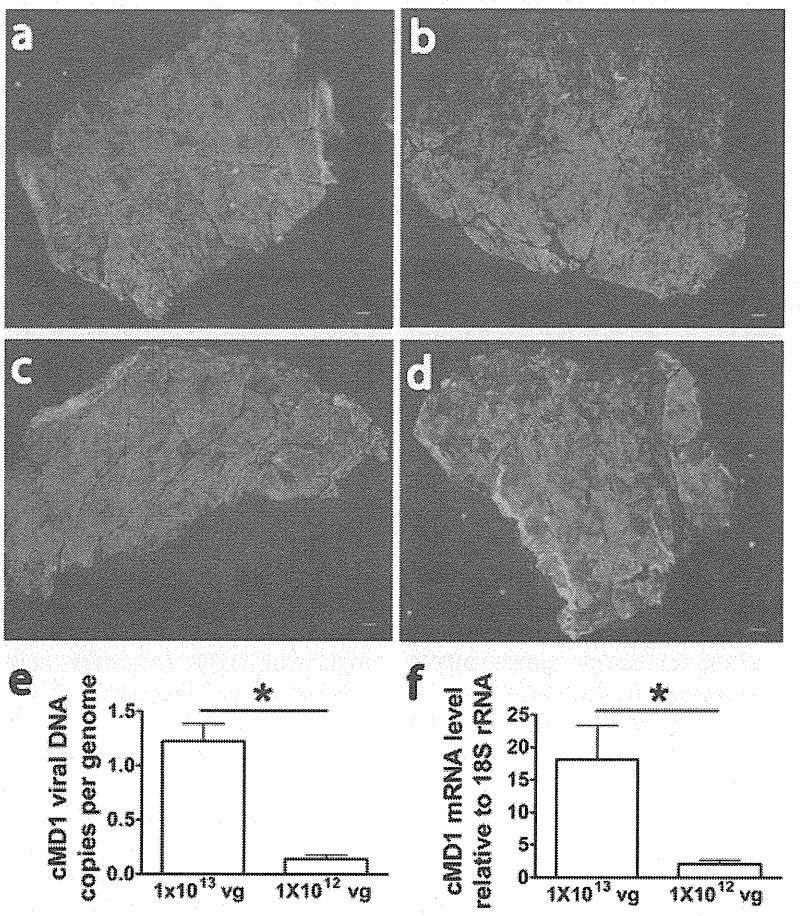

Figure 1. Widespread expression of an mRNA sequence-optimized canine microdystrophin after intramuscular injection of AAV2/8-cMD1 in the *CXMDj* muscles. The TC (a, b), ECR (c) and GC (d) muscles of the *CXMDj* dog were injected intramuscularly with either 1×10^{13} (a, c), 1×10^{12} (b) or 2×10^{13} vector genomes (d) of AAV2/8-cMD1. At 4 weeks (c) or 8 weeks (a, b and d) after injection, dystrophin expression was evaluated by immunohistochemistry using NCL-dysB antibody. Dystrophin signal was visualized with Alexafluor 568-conjugated anti-mouse IgG antibody. Scale bar = 300 μm. Microdystrophin viral DNA and transcribed mRNA were determined in TC muscles of the *CXMDj* dog at 8 weeks after injection with 1×10^{13} or 1×10^{12} vector genomes of AAV2/8-cMD1. DNA and mRNA were isolated from three random TC muscle areas. DNA (e) and mRNA (f) levels of cMD1 were evaluated by Q-PCR and Q-RT-PCR and normalized against the single copy UCR gene and 18S ribosomal RNA, respectively.

30 s) followed by 50 cycles of 95 °C for 5 s, 60 °C for 20 s with a single fluorescence measurement melting curve program (55–95 °C with heating at 0.5 °C/10 s) and continuous fluorescence measurement.

Detection of microdystrophin mRNA in muscle tissues

Approximately 20 mg of cryosections of the tissue were prepared and homogenized and RNA was extracted using RNEasy Fibrous Tissue Mini kit (Qiagen). cDNA from extracted RNA was synthesized using a Quanti-Tect Reverse Transcription kit (Qiagen). Q-PCR was performed with same protocol for detection of genomic DNA. As an internal control, 18S ribosomal RNA was used to normalize the mRNA concentration using primers (5′ to 3′): ACCGCAGCTAGGAATAATGGAA (forward) and CCTCCGACTTTCGTTCTTGATT (reverse).

Results

A single intramuscular injection of AAV2/8 vector expressing an mRNA sequence-optimized canine microdystrophin (cMD1) results in widespread and stable transgene expression in the *CXMDj* dog

To evaluate the transduction efficiency of AAV2/8 vectors carrying an mRNA sequence-optimized canine microdystrophin cDNA (cMD1), TC, ECR and GC muscles of 9-week-old male *CXMDj* dog were intramuscularly injected with either 1×10^{13} or 1×10^{12} (TC; Figures 1a and 1b), 1×10^{13} (ECR; Figure 1c) or 2×10^{13} vector genomes (GC; Figure 1d) of AAV2/8-cMD1. The ECR, TC and GC muscles were collected at 4 weeks (ECR) and 8 weeks (TC and GC). Dystrophin positive fibers in muscles injected with AAV2/8-cMD1 were counted and the

relative level of dystrophin-positive fibers was determined by morphometric evaluation of some 3000 fibers in the AAV-treated muscles and represented as a percentage of the total fiber number (Table S1).

Remarkable expression of cMD1 positive myofibers was observed in all injected muscles at both time points. Importantly, vector distribution was evident throughout the injected muscles (Figure S2). As shown in Figures 1a and 1b, TC muscles injected with 1×10^{13} or 1×10^{12} vector genomes of AAV2/8-cMD1 yielded efficient dystrophin expression, displaying 2514 and 2486 dystrophin positive fibers (corresponding to 83.6% and 70.8% of the fibers) at 8 weeks post-injection, respectively. Similar high levels of microdystrophin expression were observed in ECR and GC muscles (Figures 1c and 1d), displaying 2972 and 1635 dystrophin positive fibers (corresponding to 86.3% and 53.8% of the fibers) at 4 and 8 weeks post-injection, respectively. No detectable cMD1 expression was shown in the liver and heart of the AAV2/8-cMD1 injected *CXMDj* dog (Figure S3).

To evaluate the levels of vector-derived cMD1 DNA and mRNA in TC muscles injected with AAV2/8-cMD1, we performed quantification of viral vector genomes and mRNA levels of cMD1 at 8 weeks after injection by either Q-PCR or Q-reverse transcriptase (RT)-PCR analyses, respectively. The level of cMD1 vector copies per cellular genome was 1.2 and 0.14 in samples from TC muscles injected with 1×10^{13} and 1×10^{12} vector genomes of AAV2/8-cMD1, respectively (DNA level normalized to that of the UCR housekeeping gene) (Figure 1e). In the case of vector transgene-derived mRNA, levels of 18-fold and two-fold compared to ribosomal 18S RNA were observed in samples of TC muscles injected with 1×10^{13} and 1×10^{12} vector genomes of AAV2/8-cMD1, respectively (Figure 1f). The ratio of AAV2/8-cMD1 mRNA to vector DNA in both the 1×10^{13} and 1×10^{12} vector genome of AAV2/8-cMD1 injected TC muscles was very similar (approximately 15), indicating that intramuscular administration of AAV2/8-cMD1 renders robust skeletal muscle mRNA expression.

Expression of canine microdystrophin from AAV2/8-cMD1 improves muscle pathology in the *CXMDj* dog

We further investigated whether microdystrophin expression can restore the muscle integrity. Lack of dystrophin in *CXMDj* dogs invariably leads to a significant loss of muscle integrity, as assessed by permeable staining for ingress of circulating endogenous blood proteins such as albumin, IgG and IgM [23]. Membrane integrity of cMD1 positive fibers was examined using anti-canine IgG antibody to detect intracellular IgG in AAV2/8-cMD1 transduced TC and GC muscles of the *CXMDj* dog. Microdystrophin positive fibers did not exhibit cytoplasmic IgG staining (0.3% of dystrophin positive fibers were IgG positive, whereas 8.3% of all fibers were IgG positive) in AAV2/8-cMD1 injected TC muscle, which indicates that the integrity of sarcolemmal membrane was improved by microdystrophin expression (Figure 2). However, very few dystrophin positive fibers in AAV2/8-cMD1 injected GC muscle showed cytoplasmic IgG staining (1.1% of dystrophin positive fibers were IgG positive, whereas 7.2% of all fibers were IgG positive), revealing that some of cMD1 positive fibers in GC muscle may not express sufficient dystrophin level to restore membrane integrity despite a relatively high (58%) cMD1 expression (Figure 2).

Next, we examined whether cMD1 expression in the *CXMDj* dog muscles can prevent or halt the muscle damage. Central nucleation is one of the markers of myofiber regeneration in dystrophic muscles. Very low central nucleation was evident in dystrophin positive fibers of AAV2/8-cMD1 injected TC muscle, which exhibited very similar histology to wild-type muscle (Figure 3). Centrally nucleated fibers were counted in four random section areas of AAV2/8-cMD1 injected and age-matched TC muscle of *CXMDj* negative control. Approximately 1.8% (±0.38%) central nucleation was observed and there was no evidence of a cellular infiltrate in TC muscle injected with AAV2/8-cMD1, whereas 9.8% (±2.28%) and 0.6% (±0.15%) of myofibers were central nucleated in age-matched TC muscle of the *CXMDj* negative control and wild-type dog, respectively (Figure 3).

Canine microdystrophin from AAV2/8-cMD1 correctly interacts with components of the associated DPC at the sarcolemmal membrane in the *CXMDj* dog

Dystrophin expressed at the sarcolemma in normal muscle associates with the DPC to form a transmembrane link that acts as a mediator of interaction and signaling between the extracellular matrix and cytoskeleton in muscle fibers [24,25]. We tested the ability of cMD1 to correctly co-localize and restore the association of DPC at the sarcolemma in the *CXMDj* dog. At 8 weeks after intramuscular injection of 1×10^{13} vector genomes of AAV2/8-cMD1, co-localization of DPC components such as α-dystrobrevin and α1-syntrophin were observed in microdystrophin positive fibers in the TC muscles (Figure 4).

Reduction of inflammatory responses in muscles after intramuscular injection of AAV2/8-cMD1

To evaluate the inflammatory lesions in muscles, we evaluated the $CD8^+$ T-cell mediated immune responses in the ECR, TC and GC muscle at 4 (ECR) and 8 weeks (TC and GC) after intramuscular injection of AAV2/8-cMD1. There were very few $CD8^+$ T-cells observed in AAV2/8-cMD1 injected muscles, whereas saline injected age-matched TC muscle of the *CXMDj* dog showed widespread $CD8^+$ T-cell infiltration (Figure 5). No cellular infiltration was shown in age-matched wild-type TC muscle.

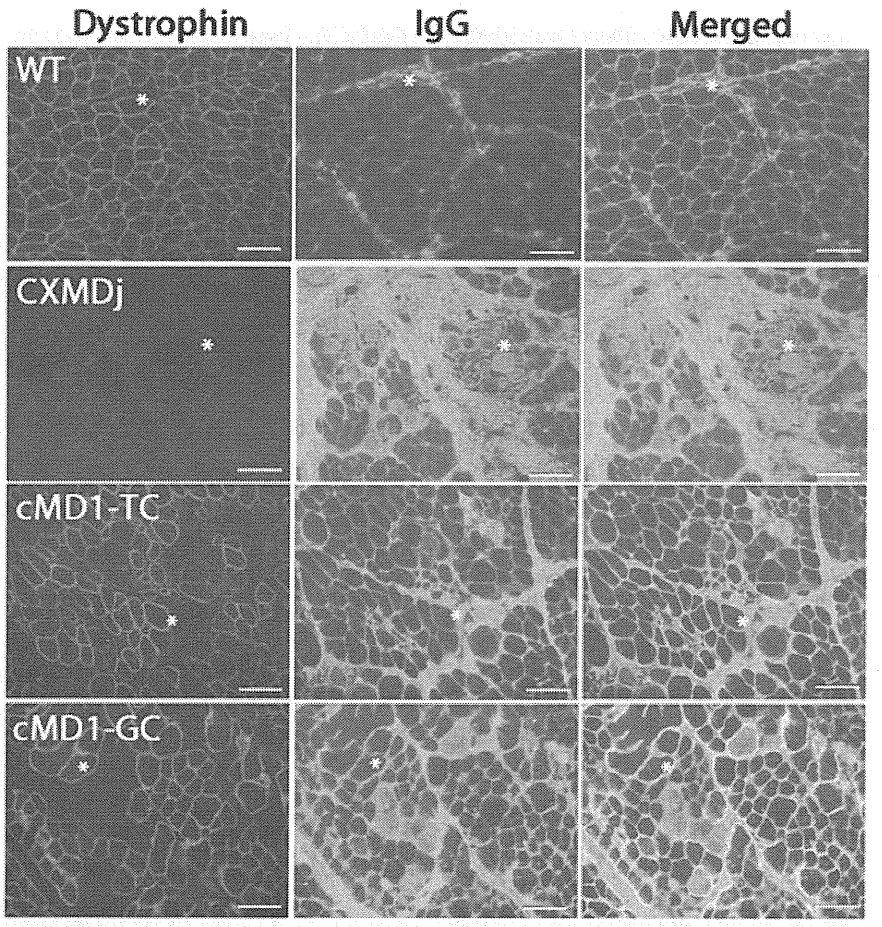

Figure 2. Examination of membrane integrity of the *CXMDj* dog muscles after intramuscular injection of AAV2/8-cMD1. The TC or GC muscles of the *CXMDj* dog were injected with either 1×10^{13} or 2×10^{13} vector genomes of AAV2/8-cMD1, respectively. At 8 weeks post injection, tissues were harvested, cryosectioned and subjected to immunohistology of serial sections to examine membrane integrity. Serial sections were stained using NCL-dysB antibody against dystrophin or an Alexafluor 488-anti-canine IgG antibody. The dystrophin signal was visualized with an Alexafluor 568-conjugated anti-mouse IgG. The right-hand panel shows the merged images for dystrophin and anti-canine IgG. Age-matched TC muscles of wild-type (WT) and *CXMDj* dog were assessed in parallel as positive and negative controls, respectively. Scale bar = 50 μm.

Discussion

In the present study, we demonstrated that a single intramuscular injection of AAV2/8 expressing an mRNA sequence-optimized canine specific microdystrophin yields high and stable levels of microdystrophin expression in the *CXMDj* dog model. Previously, it has been demonstrated that mRNA sequence-optimization increased microdystrophin expression dramatically after systemic administration of the AAV2/8 vectors in the neonatal *mdx* mouse model [13]. These high levels of mRNA sequence-optimized microdystrophin expression lead to a significant improvement of muscle function and specific muscle force in *mdx* mice [13].

cMD1 expression was regulated by the highly-active muscle specific synthetic promoter, SPc5-12, which has been reported to be six- to eight-fold stronger than the CMV promoter in the skeletal muscle of immunocompetent mice [19]. No detectable cMD1 expression was shown in the liver and heart of AAV2/8-cMD1 injected the *CXMDj* dog, demonstrating that cMD1 expression is regulated by the transcriptional control of a muscle-synthetic promoter (SPc5-12). Administration of AAV2/8 expressing cMD1 resulted in correct localization of α-dystrobrevin and α1-syntrophin, which form part of the DPC at the sarcolemma. Interestingly, this phenomenon can occur even in the absence of the C-terminal domain of dystrophin, which has binding sites for α-dystrobrevin and α1-syntrophin [24,25], demonstrating that cMD1 can interact with α-dystrobrevin and α1-syntrophin independently of the C-terminal domain of dystrophin. This result supports the findings of a previous study showing that α1-syntrophin and α-dystrobrevin can bind to dystrophin even in the absence of the C-terminal domain of dystrophin [26].

A major hurdle facing AAV-mediated gene therapy is the ability to avoid immune responses to both the vector (which would inhibit the ability to re-administer vector) and

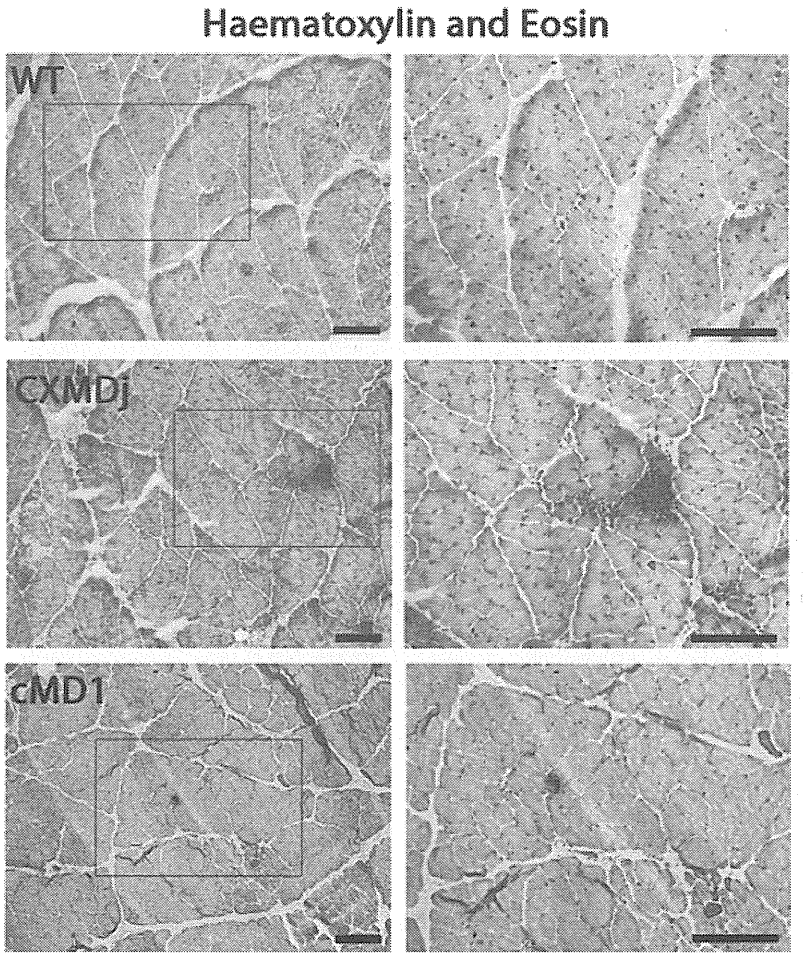

Figure 3. Central nucleation after AAV2/8-cMD1 injection into TC muscles of the *CXMDj* dog. The TC muscle of the *CXMDj* dog was injected with 1×10^{13} vector genomes of AAV2/8-cMD1. At 8 weeks after injection, tissues were harvested, cryosectioned and subjected to immunohistological analysis. Cross-sections were stained with H&E. Age-matched TC muscles of wild-type (WT) and *CXMDj* dog were assessed in parallel as positive and negative controls, respectively. Central nucleated fibers were counted under × 100 magnification in five selected fields Left: × 100 magnification, Right: × 200 magnification. Scale bar = 100 μm.

immune-mediated clearance of novel dystrophin proteins. Such safety concerns came to the forefront subsequent to the use of AAV vectors in large animal models and human clinical trials. T-cell mediated immune responses against AAV2 capsid protein were demonstrated after intra-hepatic delivery of AAV2 in a phase I/II clinical trial of haemophilia B [27]. Recently, a clinical trial was conducted in six DMD patients in whom AAV vectors expressing human microdystrophin were injected intramuscularly and dystrophin specific T-cells were detected [18]. Importantly, of the six treated patients, two subjects appeared to exhibit pre-existing dystrophin specific T-cells, possibly reacting against rare dystrophin-positive revertant fibers, in peripheral blood mononuclear cells before treatment [18]. Similarly, immune responses to both vector and transgene have been observed in dog models after AAV gene transfer [10,11,14,15]. It has been demonstrated that AAV2 and AAV8 are associated with humoral immune responses in muscular dystrophy dogs [14]. In addition, an inflammatory response and growth retardation have recently been described after systemic administration of a high-dose AAV2/9 expressing human minidystrophin under the control of the CMV promoter in neonatal GRMD dogs [28]. Despite these issues, high levels of human minidystrophin expression were seen up to 16 weeks post-administration [28]. It was suggested that this may be a result of the immature nature of the immune system of neonatal dogs. Previous studies using AAV2/6 vectors encoding a nonsequence-optimized, human-specific microdystrophin (ΔR4-23/ΔCT) under a CMV promoter resulted in the limited expression and eventual destruction of injected *CXMDj* dog muscle fibers via the immune system at 6 weeks after discontinuation of immunosuppression, 22 weeks after initial intramuscular injection [29]. It is important to note that we observed widespread microdystrophin (ΔR4–23/ΔCT; called cMD1) expression for up to 8 weeks after injection into multiple skeletal muscles of juvenile *CXMDj* dog in the absence of immunosuppression.

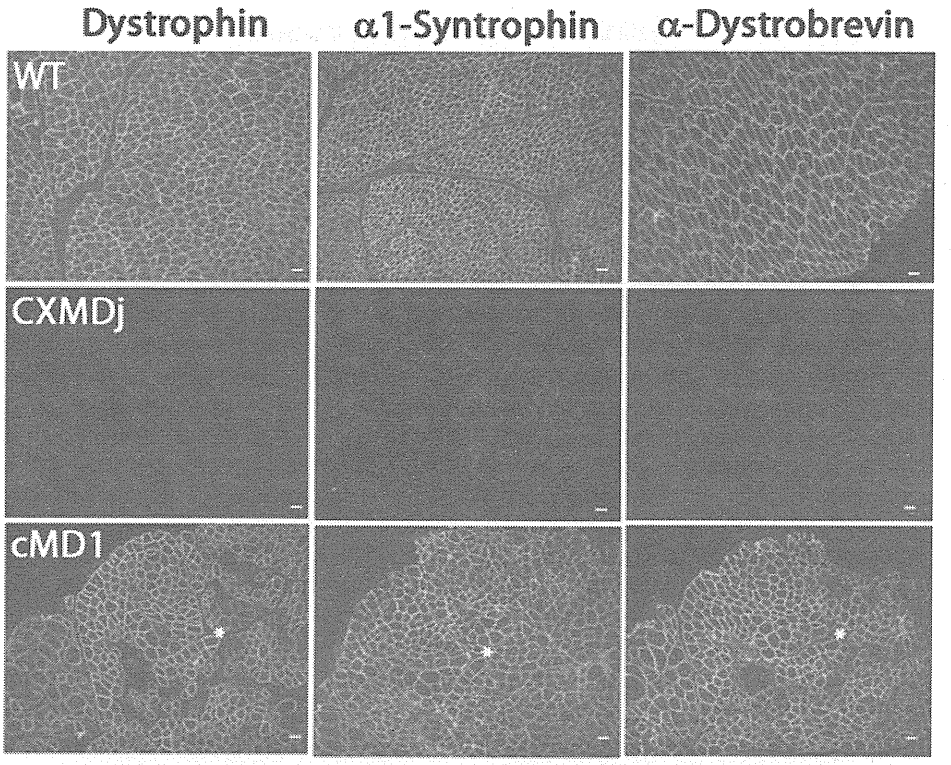

Figure 4. Co-localization of dystrophin and the DPC in TC muscles of microdystrophin treated *CXMDj* dog. TC muscle of the *CXMDj* dog was injected with 1×10^{13} vector genomes of AAV2/8-cMD1. Tissues were harvested 8 weeks later and serial sections were stained using antibodies for dystrophin, α-dystrobrevin and α1-syntrophin to examine co-localization of these proteins at the sarcolemma. The dystrophin and α-dystrobrevin signals were visualized with Alexafluor 568-conjugated anti-mouse IgG. The α1-syntrophin signal was visualized with Alexafluor 568-conjugated anti-rabbit IgG. Age-matched TC muscles of wild-type (WT) and *CXMDj* dog were assessed in parallel as positive and negative controls, respectively. Scale bar = 50 μm.

H&E staining shows no evidence of inflammation, which would be an indicator of an ongoing immune response. It also shows very low levels of central nucleation, suggesting that the muscle is not undergoing regeneration as a result of either a transgene-specific immune response or poor functionality of the microdystrophin. In addition, no apparent $CD8^+$ T-cell mediated immune responses in the AAV2/8-cMD1 injected *CXMDj* muscle suggest that cMD1 expression may inhibit inflammation. No cytoplasmic IgG staining was observed in cMD1 positive myofibers in TC muscle at 8 weeks after injection, suggesting that cMD1 expression can improve the integrity of the sarcolemma in TC muscles. However, cMD1 failed to protect membrane integrity in very few cMD1 positive myofibers in GC muscles. This may be a result of the insufficient expression of cMD1 in several fibers in large volume GC muscles.

In summary, we demonstrate, for the first time, that the delivery of AAV2/8 carrying an mRNA sequence-optimized canine specific microdystrophin under the control of muscle-specific promoter into the *CXMDj* muscles can lead to high expression of functional microdystrophin, without the need for an immunomodulation/suppression regimen. The present study provides important data on the sequence/species optimization and tissue-specific restriction of microdystrophin, demonstrating that it can increase mRNA and protein expression levels and restore DPC association at the sarcolemma, leading to muscle protection in a 16-week-old *CXMDj* dog model of DMD. The development of AAV2/8-mediated gene transfer of highly functional microdystrophin in a canine model of DMD may contribute to facilitating its successful application to gene therapy clinical trials for DMD. This meets the objective of developing safe and effective muscle gene therapy protocols that are appropriate for moving forward towards clinical trials. The systemic delivery of mRNA sequence-optimized microdystrophin using AAV2/8 or other suitable vectors and muscle-restricted transcription in large animal models such as dogs and nonhuman primates aiming to examine the modulation of immune responses could be the next step before implementing clinical trials in DMD patients.

Acknowledgements

The authors thank Jin-Hong Shin who performed the AAV injection. We would like to thank Dr Ruxandra Draghia-Akli for supplying the SPc5-12 promoter. This work was supported by grants from Daiwa grant Foundation, Clinigene European Network of Excellence, Duchenne Ireland and the Muscular Dystrophy Campaign. The authors declare that they have no conflicts of interest.

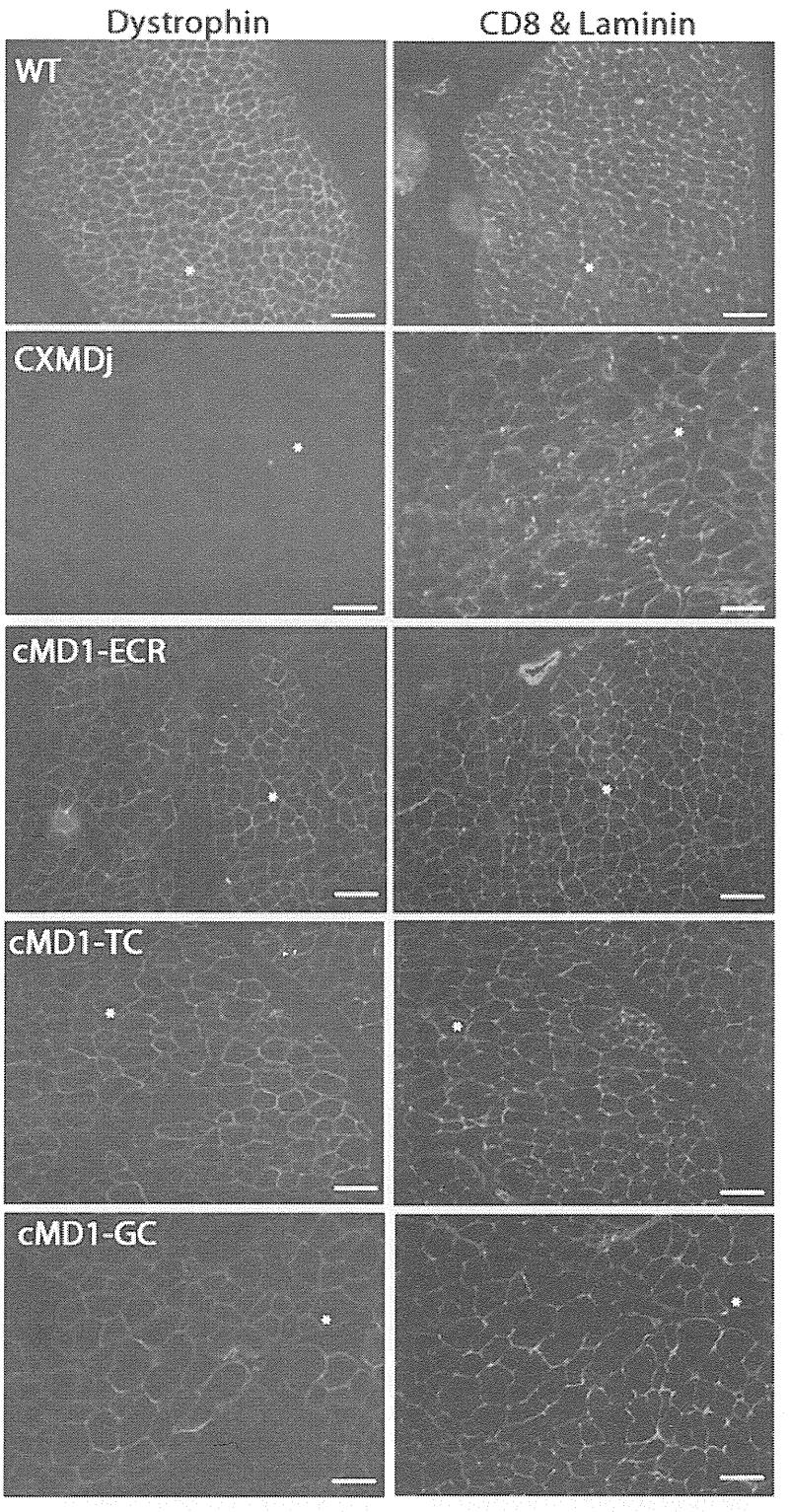

Figure 5. Inflammatory response in the *CXMDj* dog muscles after intramuscular injection of AAV2/8-cMD1. The ECR, TC and GC muscles of the *CXMDj* dog were injected with either 1×10^{13} (ECR and TC) or 2×10^{13} vector genomes (GC) of AAV2/8-cMD1. Muscles were harvested at 4 weeks (ECR) or 8 weeks (TC and GC) after injection and subjected to immunohistological analysis. Serial sections were stained for dystrophin (left-hand panel). The right-hand panel shows the merged images for mouse anti-canine CD8 (green) and rabbit anti-laminin (red). Age-matched TC muscles of wild-type (WT) and *CXMDj* dog were assessed in parallel as positive and negative controls, respectively. Scale bar = 50 μm.

References

1. Emery AEH, Muntoni F. *Duchenne muscular dystrophy*. Oxford University Press: Oxford, 2003.
2. Muntoni F, Torelli S, Ferlini A. Dystrophin and mutations: one gene, several proteins, multiple phenotypes. *Lancet Neurol* 2003; **2**: 731–740.
3. Whitehead NP, Yeung EW, Allen DG. Muscle damage in mdx (dystrophic) mice: role of calcium and reactive oxygen species. *Clin Exp Pharmacol Physiol* 2006; **33**: 657–662.
4. Neri M, Torelli S, Brown S, *et al.* Dystrophin levels as low as 30% are sufficient to avoid muscular dystrophy in the human. *Neuromuscul Disord* 2007; **17**: 913–918.
5. Gregorevic P, Blankinship MJ, Allen JM, Chamberlain JS. Systemic microdystrophin gene delivery improves skeletal muscle structure and function in old dystrophic mdx mice. *Mol Ther* 2008; **16**: 657–664.
6. Fabb SA, Wells DJ, Serpente P, Dickson G. Adeno-associated virus vector gene transfer and sarcolemmal expression of a 144 kDa micro-dystrophin effectively restores the dystrophin-associated protein complex and inhibits myofibre degeneration in nude/mdx mice. *Hum Mol Genet* 2002; **11**: 733–741.
7. Athanasopoulos T, Graham IR, Foster H, Dickson G. Recombinant adeno-associated viral (rAAV) vectors as therapeutic tools for Duchenne muscular dystrophy (DMD). *Gene Ther* 2004; **11**(Suppl 1): S109–S121.
8. Lai Y, Thomas GD, Yue Y, *et al.* Dystrophins carrying spectrin-like repeats 16 and 17 anchor nNOS to the sarcolemma and enhance exercise performance in a mouse model of muscular dystrophy. *J Clin Invest* 2009; **119**: 624–635.
9. Wu Z, Yang H, Colosi P. Effect of genome size on AAV vector packaging. *Mol Ther* 2010; **18**: 80–86.
10. Wang Z, Allen JM, Riddell SR, *et al.* Immunity to adeno-associated virus-mediated gene transfer in a random-bred canine model of Duchenne muscular dystrophy. *Hum Gene Ther* 2007; **18**: 18–26.
11. Yuasa K, Yoshimura M, Urasawa N, *et al.* Injection of a recombinant AAV serotype 2 into canine skeletal muscles evokes strong immune responses against transgene products. *Gene Ther* 2007; **14**: 1249–1260.
12. Yoshimura M, Sakamoto M, Ikemoto M, *et al.* AAV vector-mediated microdystrophin expression in a relatively small percentage of mdx myofibers improved the mdx phenotype. *Mol Ther* 2004; **10**: 821–828.
13. Foster H, Sharp PS, Athanasopoulos T, *et al.* Codon and mRNA sequence optimization of microdystrophin transgenes improves expression and physiological outcome in dystrophic mdx mice following AAV2/8 gene transfer. *Mol Ther* 2008; **16**: 1825–1832.
14. Ohshima S, Shin JH, Yuasa K, *et al.* Transduction efficiency and immune response associated with the administration of AAV8 vector into dog skeletal muscle. *Mol Ther* 2009; **17**: 73–80.
15. Pichavant C, Chapdelaine P, Cerri DG, *et al.* Expression of dog microdystrophin in mouse and dog muscles by gene therapy. *Mol Ther* 2010; **18**: 1002–1009.
16. Blankinship MJ, Gregorevic P, Allen JM, *et al.* Efficient transduction of skeletal muscle using vectors based on adeno-associated virus serotype 6. *Mol Ther* 2004; **10**: 671–678.
17. Riviere C, Danos O, Douar AM. Long-term expression and repeated administration of AAV type 1, 2 and 5 vectors in skeletal muscle of immunocompetent adult mice. *Gene Ther* 2006; **13**: 1300–1308.
18. Mendell JR, Campbell K, Rodino-Klapac L, *et al.* Dystrophin immunity in Duchenne's muscular dystrophy. *N Engl J Med* 2010; **363**: 1429–1437.
19. Li X, Eastman EM, Schwartz RJ, Draghia-Akli R. Synthetic muscle promoters: activities exceeding naturally occurring regulatory sequences. *Nat Biotechnol* 1999; **17**: 241–245.
20. Okada T, Nomoto T, Yoshioka T, *et al.* Large-scale production of recombinant viruses by use of a large culture vessel with active gassing. *Hum Gene Ther* 2005; **16**: 1212–1218.
21. Okada T, Nonaka-Sarukawa M, Uchibori R, *et al.* Scalable purification of adeno-associated virus serotype 1 (AAV1) and AAV8 vectors, using dual ion-exchange adsorptive membranes. *Hum Gene Ther* 2009; **20**: 1013–1021.
22. Bejerano G, Pheasant M, Makunin I, *et al.* Ultraconserved elements in the human genome. *Science* 2004; **304**: 1321–1325.
23. Blake DJ, Weir A, Newey SE, Davies KE. Function and genetics of dystrophin and dystrophin-related proteins in muscle. *Physiol Rev* 2002; **82**: 291–329.
24. Campbell KP. Three muscular dystrophies: loss of cytoskeleton-extracellular matrix linkage. *Cell* 1995; **80**: 675–679.
25. Tinsley JM, Blake DJ, Zuellig RA, Davies KE. Increasing complexity of the dystrophin-associated protein complex. *Proc Natl Acad Sci USA* 1994; **91**: 8307–8313.
26. Crawford GE, Faulkner JA, Crosbie RH, Campbell KP, Froehner SC, Chamberlain JS. Assembly of the dystrophin-associated protein complex does not require the dystrophin COOH-terminal domain. *J Cell Biol* 2000; **150**: 1399–1410.
27. Manno CS, Pierce GF, Arruda VR, *et al.* Successful transduction of liver in hemophilia by AAV-factor IX and limitations imposed by the host immune response. *Nat Med* 2006; **12**: 342–347.
28. Kornegay JN, Li J, Bogan JR, *et al.* Widespread muscle expression of an AAV9 human mini-dystrophin vector after intravenous injection in neonatal dystrophin-deficient dogs. *Mol Ther* 2010; **18**: 1501–1508.
29. Wang Z, Kuhr CS, Allen JM, *et al.* Sustained AAV-mediated dystrophin expression in a canine model of Duchenne muscular dystrophy with a brief course of immunosuppression. *Mol Ther* 2007; **15**: 1160–1166.

Gene Therapy (2011), 1–10

www.nature.com/gt

ORIGINAL ARTICLE

Improvement of cardiac fibrosis in dystrophic mice by rAAV9-mediated *microdystrophin* transduction

J-H Shin, Y Nitahara-Kasahara, H Hayashita-Kinoh, S Ohshima-Hosoyama, K Kinoshita, T Chiyo, H Okada, T Okada and S Takeda

Duchenne muscular dystrophy (DMD) is the most common form of the progressive muscular dystrophies characterized by defects of the *dystrophin* gene. Although primarily characterized by degeneration of the limb muscles, cardiomyopathy is a major cause of death. Therefore, the development of curative modalities such as gene therapy is imperative. We evaluated the cardiomyopathic features of *mdx* mice to observe improvements in response to intravenous administration of recombinant adeno-associated virus (AAV) type 9 encoding *microdystrophin*. The myocardium was extensively transduced with *microdystrophin* to significantly prevent the development of fibrosis, and expression persisted for the duration of the study. Intraventricular conduction patterns, such as the QRS complex duration and S/R ratio in electrocardiography, were also corrected, indicating that the transduced *microdystrophin* has a protective effect on the dystrophin-deficient myocardium. Furthermore, BNP and ANP levels were reduced to normal, suggesting the absence of cardiac dysfunction. In aged mice, prevention of ectopic beats as well as echocardiographic amelioration was also demonstrated with improved exercise performance. These findings indicate that AAV-mediated cardiac transduction with *microdystrophin* might be a promising therapeutic strategy for the treatment of dystrophin-deficient cardiomyopathy.
Gene Therapy advance online publication, 31 March 2011; doi:10.1038/gt.2011.36

Keywords: Duchenne muscular dystrophy; cardiomyopathy; AAV vector; microdystrophin; electrocardiography; cardiac fibrosis

INTRODUCTION

Duchenne muscular dystrophy (DMD) is a devastating X-linked inherited disease and the most frequent form of progressive muscular dystrophy, affecting roughly 1 in 3500 male births.[1] DMD is caused by a variety of mutations in the *dystrophin* gene.[2] Often overshadowed by the manifestation of limb muscle weakness, cardiomyopathy afflicts almost all patients with DMD,[3] and is a major cause of death from this disease.[4] Cardiomyopathy is also prevalent in Becker muscular dystrophy (BMD), which is a milder form of muscular dystrophy also caused by defects in the *dystrophin* gene. Although the progression of BMD is slower than that of DMD, the symptoms of cardiac failure may be more severe in BMD than in DMD due to the greater functional demands placed on the heart by persistent patient mobility.[5] At the onset of refractory congestive heart failure, these patients become candidates for heart transplantation[6] and alternative treatment options are limited to corticosteroid or symptomatic therapy.

Recombinant adeno-associated viruses (rAAV) are promising gene transfer vectors with no known pathogenicity.[7] However, *dystrophin* is the largest human gene identified to date and its cDNA measures ~14 kb,[8] well beyond the packaging capacity of rAAV.[9] Therefore, *microdystrophin*, in which most of the rod domains of *dystrophin* are deleted, was developed to fit into rAAV.[10,11] We and others have reported successful improvement of the dystrophic phenotype in skeletal muscles of DMD mice models following introduction of this transgene.[12,13] To achieve transduction of an entire extremity, a limb perfusion by retrograde intravenous administration of the rAAV in larger animal models is being developed.[14] For cardiac transduction, we utilized rAAV serotype 9, which can be administered systemically with excellent cardiac tropism.[15]

In this study, we used *mdx* mice which are considered to be a representative animal model of DMD.[16] They lack full-length dystrophin in their muscles, due to a nonsense mutation in exon 23 of the *dystrophin* gene.[17,18] The *mdx* mice show initial evidence of cardiac dysfunction at 8–12 weeks,[19] and develop moderate myocardial necrosis and fibrosis by 6–8 months of age,[20] which progresses continuously thereafter. Correction of basic electrocardiographic (ECG) profiles was suggested after *microdystrophin* transduction in neonatal *mdx* mice,[21] although limited hemodynamic improvement was observed following *microdystrophin* transduction.[22] Here, we explored rAAV9-mediated myocardial *microdystrophin* transduction for the prevention of cardiac pathology as well as dysfunction. Long-term extensive cardiac transduction with *microdystrophin* demonstrated successful improvement of cardiac fibrosis with amelioration of DMD cardiomyopathy.

RESULTS

Extensive long-term expression of microdystrophin by rAAV9-mediated transduction

Transduction of the *mdx* mice with the rAAV9 containing CMV promoter and *microdystrophin* were evaluated, following administration of the vector at 3.0×10^{12} viral genomes/mouse via the tail vein at

Department of Molecular Therapy, National Institute of Neuroscience, National Center of Neurology and Psychiatry, Kodaira, Tokyo, Japan
Correspondence: Dr T Okada or Dr S Takeda, Department of Molecular Therapy, National Institute of Neuroscience, National Center of Neurology and Psychiatry, 4-1-1 Ogawa-higashi, Kodaira, Tokyo 187-8502, Japan.
E-mails: t-okada@ncnp.go.jp or takeda@ncnp.go.jp
Received 16 August 2010; revised 3 January 2011; accepted 3 January 2011

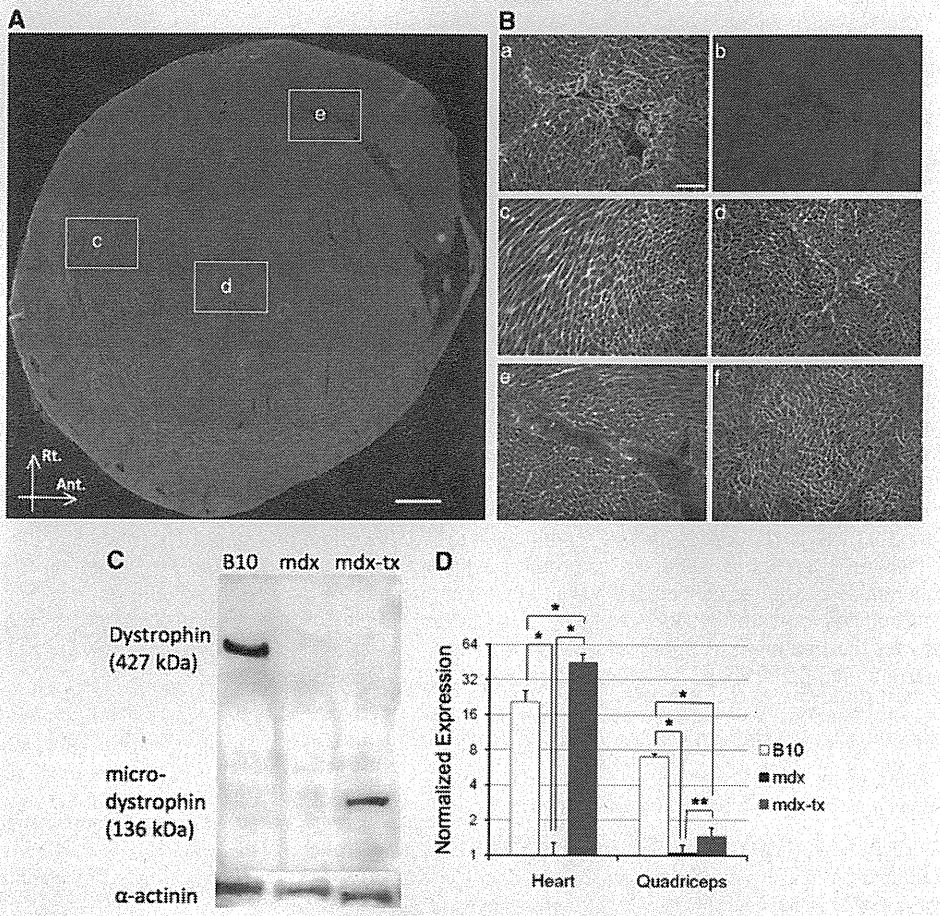

Figure 1 Expression of dystrophin/microdystrophin in cardiac muscles. (**A**) Transverse section of *mdx* mouse heart at mid-ventricular level 24 weeks after transduction of *microdystrophin*, stained with anti-dystrophin antibody NCL-DysB. Scale bar, 500 μm. (**B**) Expression of dystrophin in C57BL10 hearts at the sarcolemma (a), while it is absent in *mdx* hearts (b). Magnified views of sections from the center of the left ventricle at 28 weeks (c–e) show microdystrophin expression in the areas indicated in (**A**) (scale bar, 100 μm). At 74 weeks after transduction, *mdx* mice still retain extensive expression of microdystrophin (f). (**C**) In Western blot analysis of hearts at 28 weeks old, dystrophin is detected in the C57BL10 mice (B10), while microdystrophin is detected in the transduced *mdx* mice (mdx-tx). (**D**) *Dystrophin/microdystrophin* mRNA expression levels in the heart or quadriceps of 28-week-old C57BL10, untransduced *mdx*, and transduced *mdx* mice were measured by quantitative RT–PCR (n=3 per group). mRNA levels were normalized to 18S rRNA. $^{*}P<0.01$; $^{**}P<0.05$.

4 weeks of age. The microdystrophin contains the N-terminal, actin-binding domain, four rod repeats (R1, 2, 3, 24) and three hinges (H1, 2, 4), the cysteine-rich domain, and the truncated C-terminal domain.[12] Intravenous systemic delivery of the rAAV9-*microdystrophin* effectively transduced the cardiac tissue of *mdx* mice, and the expression of *microdystrophin* persisted until they were killed at 24 (Figures 1A and Bc–e) or 74 weeks (Figure 1Bf) after transduction. A large percentage of cardiomyocytes were transduced in both ventricles, with no difference in the number of transduced cardiomyocytes between endomyocardial and epimyocardial tissues. Immunofluorescence microscopy revealed that expressed microdystrophin localized at the sarcolemma of cardiomyocytes (Figure 1Bc–f).

We also examined the expression of dystrophin in C57BL10 mice and microdystrophin in the transduced *mdx* mice by western blot analysis (Figure 1C), and the expression levels of *dystrophin/microdystrophin* mRNA in the heart and quadriceps muscle by quantitative RT–PCR (n=3 per group, Figure 1D). The amount of microdystrophin expression in the transduced cardiac tissue of the *mdx* mice came near to the level of dystrophin expression in C57BL10 mice. In contrast, expression level of *dystrophin/microdystrophin* mRNA in the untransduced *mdx* mice was negligible. In quadriceps, the copy number of *microdystrophin* mRNA in transduced *mdx* mice was significantly lower than that of *dystrophin* in C57BL10 mice (n=3 per group, Figure 1D) and the expression of *microdystrophin* in the skeletal muscle was marginal at 24 weeks after transduction (Supplementary Figure 1), which is below the estimated therapeutic level.

Transduced *mdx* mice do not develop sinus tachycardia or QRS abnormalities

Mice were injected with 3.0×10^{12} viral genomes/mouse via the tail vein at 4 weeks of age for periodical evaluation (n=3–4 per group at each time point). The ECG data obtained from C57BL10, untransduced *mdx* mice, and transduced *mdx* mice are summarized in Table 1. Untransduced *mdx* mice demonstrated higher heart rates and shorter PR intervals than C57BL10 mice (Figures 2a, b, d and e) at 8 weeks of age. These abnormalities persisted until the age of 28 weeks ($P<0.01$ compared with C57BL10 mice). When *mdx* mice were transduced with *microdystrophin*, their heart rates slowed and the PR intervals lengthened in comparison to those of the untransduced *mdx* mice at 4 weeks after transduction (Figures 2c–e).

Table 1 Baseline ECG parameters in C57BL10, untransduced *mdx* and transduced *mdx* mice

	C57BL10	*Untransduced* mdx	*Transduced* mdx
8 weeks old			4 weeks after transduction
HR (b.p.m.)[a,b]	512 ± 11	581 ± 9.2	533 ± 13.5
PR interval (b.p.m.)[a,c,d]	43.3 ± 0.56	36.0 ± 0.44	40.4 ± 0.73
QRS duration (ms)	8.82 ± 0.23	9.08 ± 0.29	8.79 ± 0.13
S/R ratio[a,e]	0.703 ± 0.071	0.365 ± 0.069	0.491 ± 0.062
12 weeks old			8 weeks after transduction
HR (b.p.m.)[a,c]	538 ± 7.4	590 ± 5.0	538 ± 6.4
PR interval (b.p.m.)[a,c]	44.1 ± 0.72	35.6 ± 0.41	42.05 ± 0.76
QRS duration (ms)[a,c]	8.64 ± 0.20	10.82 ± 0.47	8.95 ± 0.10
S/R ratio[a,b]	0.610 ± 0.045	0.247 ± 0.089	0.490 ± 0.076
28 weeks old			24 weeks after transduction
HR (b.p.m.)[a,c]	502 ± 14.8	568 ± 9.8	524 ± 8.3
PR interval (b.p.m.)[a,b,d]	47.7 ± 1.53	38.8 ± 0.93	41.4 ± 0.28
QRS duration (ms)[a,c]	8.81 ± 0.12	10.31 ± 0.33	8.48 ± 0.18
S/R ratio[a,c]	0.719 ± 0.069	0.112 ± 0.072	0.678 ± 0.082
76 weeks old			72 weeks after transduction
HR (b.p.m.)[b]	519 ± 23.1	484 ± 18.4	534 ± 5.3
PR interval (b.p.m.)[b,e]	46.1 ± 1.76	43.66 ± 0.91	39.51 ± 1.11
QRS duration (ms)[b]	10.22 ± 0.40	10.73 ± 0.37	9.55 ± 0.29
S/R ratio	0.405 ± 0.099	0.602 ± 0.154	0.384 ± 0.067

Abbreviations: ECG, electrocardiographic; HR, heart rate.
Values are the mean ± s.e.
[a]$P<0.01$ between C57BL10 and untransduced *mdx*.
[b]$P<0.05$ between transduced and transduced *mdx*.
[c]$P<0.01$ between transduced and transduced *mdx*.
[d]$P<0.01$ between C57BL10 and transduced *mdx*.
[e]$P<0.05$ between C57BL10 and transduced *mdx*.

Untransduced *mdx* mice also showed longer QRS durations (Figure 2f) compared with those of C57BL10 mice at 12 weeks of age ($P<0.01$), and the S/R ratios were significantly lower in untransduced *mdx* mice than in C57BL10 mice at 8 weeks of age ($P<0.01$; Figures 2a, b and g). The S/R ratio of the untransduced *mdx* mice continued to decrease with age up to 28 weeks. These QRS complex abnormalities significantly improved in transduced *mdx* mice at 28 weeks of age, and the improvements persisted for the duration of the study (Figures 2c, f and g). The improved values measured in the transduced *mdx* mice did not differ significantly from those of C57BL10 mice. The differences in ECG parameters between C57BL10 and untransduced *mdx* mice were diminished in mice at 76 weeks old.

Parasympathetic influence determines the difference in heart rate between normal and dystrophic mice

Heart rate and PR interval changed dynamically in accordance with body temperature in normal and *mdx* mice (Figure 3a). These data suggest that sinus tachycardia with a short PR interval in *mdx* mice is more likely to be a regulatory response of the autonomic nervous system than a consequence of structural abnormalities. Pharmacological blockade with the atropine treatment induced a paradoxical heart rate drop in untransduced *mdx* mice, as has been reported previously,[23] while transduced *mdx* mice exhibited a normal tachycardic response comparable to that of C57BL10 mice (n=3–4 per group at each time point, Figure 3b). In contrast, the response to propranolol was not significantly different between the groups (Figure 3c). In addition, in order to estimate the amount of sympathetic tone in the awake state, we measured the urinary excretion of catecholamine and found that the levels of epinephrine and norepinephrine were in the same range in all three groups (n=7 per group, Supplementary Figure 2). We also tested the mRNA levels of BNP and ANP in the ventricular myocardium at 24 weeks after transduction (n=3 per group). Transcripts of both peptides were significantly increased in untransduced *mdx* mice ($P<0.01$), but were decreased in the transduced *mdx* mice to levels approaching that of C57BL10 mice (Figure 4).

Transduction with *microdystrophin* prevents cardiac fibrosis in *mdx* mice

Widespread cardiac fibrosis is indicative of advanced cardiomyopathy in DMD patients. In this study, the therapeutic effect of microdystrophin was associated with reduced cardiac fibrosis (Figures 5a–f). When compared with *mdx* mice at 24 weeks after transduction, age-matched untransduced *mdx* mice showed marked infiltration of fibrosis in the cardiac tissue. Although the distribution of fibrosis varied among the mice, fibrotic changes in untransduced *mdx* mice were most prominently observed in the epimyocardial tissues of the left ventricle. Right ventricles were also infiltrated with fibrous tissue to varying degrees. In contrast, *microdystrophin* transduction of *mdx* mice successfully improved the pathologic changes in the heart muscle. The amount of fibrous tissue measured by Sirius red staining was statistically equivalent to that of C57BL10 control mice (n=3 per group, Figure 5g). Furthermore, TGF-β upregulation was prevented in the hearts of *mdx* mice at 24 weeks after *microdystrophin* transduction, while mRNA levels of TGF-β were significantly increased in the untransduced *mdx* mice (n=3 per group, Figure 5h). Long-term analysis of the cardiac fibrosis demonstrated that the untransduced *mdx* mice at 18 months after transduction showed extensive fibrosis in the epimyocardial area, while fibrosis was not evident in the transduced *mdx* mice (Supplementary Figure 4).

ECG findings in aged mice

Various ECG abnormalities appeared in untransduced *mdx* mice at 76 weeks of age. Ventricular premature contractions (VPCs) were frequently recorded in aged untransduced *mdx* mice (Figures 6a and c), while VPCs were observed only at frequencies of <1 VPC every 10 min in C57BL10 and transduced *mdx* mice at the same or younger ages. In addition, QRS complexes with a pre-excitation pattern were recorded on ECGs in half of the aged untransduced *mdx* mice (Figures 6b and c).

Dilated cardiomyopathy is prevented in transduced *mdx* mice

Left ventricular dimensions and Doppler tissue velocities were measured in 76 weeks old mice. In untransduced *mdx* mice, dilated cardiomyopathy was evident and fractional shortening was markedly reduced. In contrast, ventricular function and heart muscle structure were preserved in the transduced *mdx* mice (n=4–5 per group, Figure 7a). Systolic and diastolic Doppler tissue velocities were also significantly reduced in the untransduced *mdx* mice (n=4–5 per group, Figure 7b) compared with C57BL10 and transduced *mdx* mice.

Transduction with *microdystrophin* improves voluntary wheel running performance

To evaluate if *microdystrophin* transduction improves the exercise performance of *mdx* mice, voluntary wheel running performances of

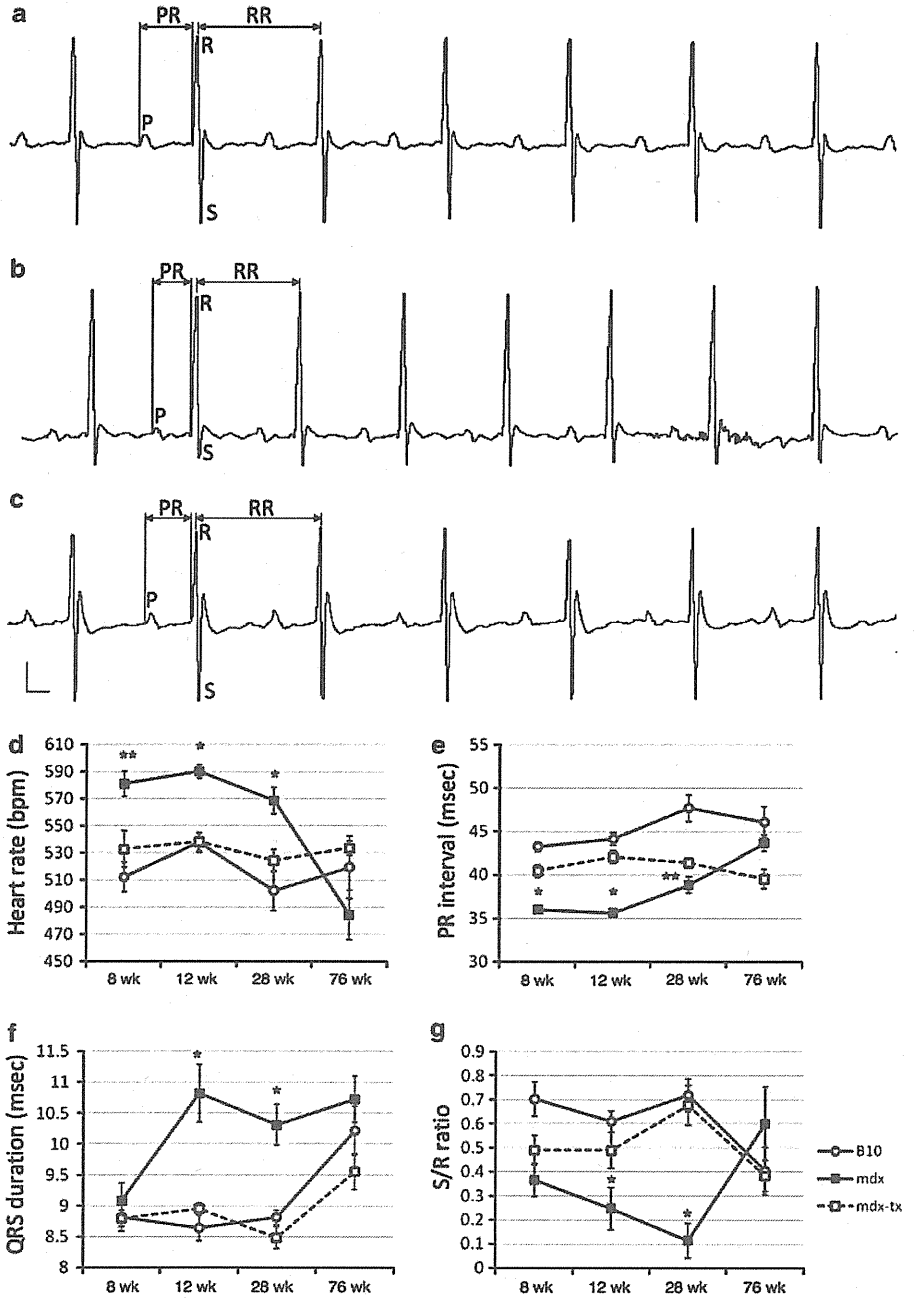

Figure 2 ECGs of C57BL10, untransduced *mdx* and transduced *mdx* mice. (**a–c**) Representative ECG tracings from mice at the age of 8 weeks. Compared with the ECG tracing of C57BL10 mice (**a**), *mdx* mice (**b**) show a shorter RR interval, a shorter PR interval, and a smaller S/R ratio. These ECG abnormalities are prevented in the transduced *mdx* mice (**c**). Vertical scale bar, 200 μV; horizontal scale bar, 20 ms. (**d–g**) Graphical representation of ECG profiles with age (n=3–4 per group at each time point); (**d**) heart rate, (**e**) PR interval, (**f**) QRS duration, and (**g**) S/R ratio. The horizontal axis represents age. C57BL10 mice (B10) are represented by open circles with solid lines, untransduced *mdx* mice (mdx) by filled squares with solid lines, and *mdx* mice transduced with *microdystrophin* (mdx-tx) by open squares with broken lines. Data are shown as mean ± s.e.m; *P<0.01 between C57BL10 mice and untransduced *mdx* mice, and also between transduced *mdx* mice and untransduced *mdx* mice; **P<0.01 between C57BL10 mice and untransduced *mdx* mice, as well as P<0.05 between transduced *mdx* mice and untransduced *mdx* mice.

the untransduced and transduced *mdx* mice were analyzed for 13 days (Figure 8). *Microdystrophin* transduction of the *mdx* mice resulted in a significant and consistent improvement of daily running distances (Figure 8a). Cumulative running distance of the *microdystrophin*-transduced *mdx* mice (Figure 8b, n=4 per group, mean 28.67 km, 2.17 km as daily running) during the 13 days was longer than that of the untransduced *mdx* mice (n=4 per group, P<0.01, unpaired t-test, mean 9.94 km, 0.76 km as daily running). The differences in cumulative running distances also reflected daily running distances between untransduced and transduced *mdx* mice. *Microdystrophin*

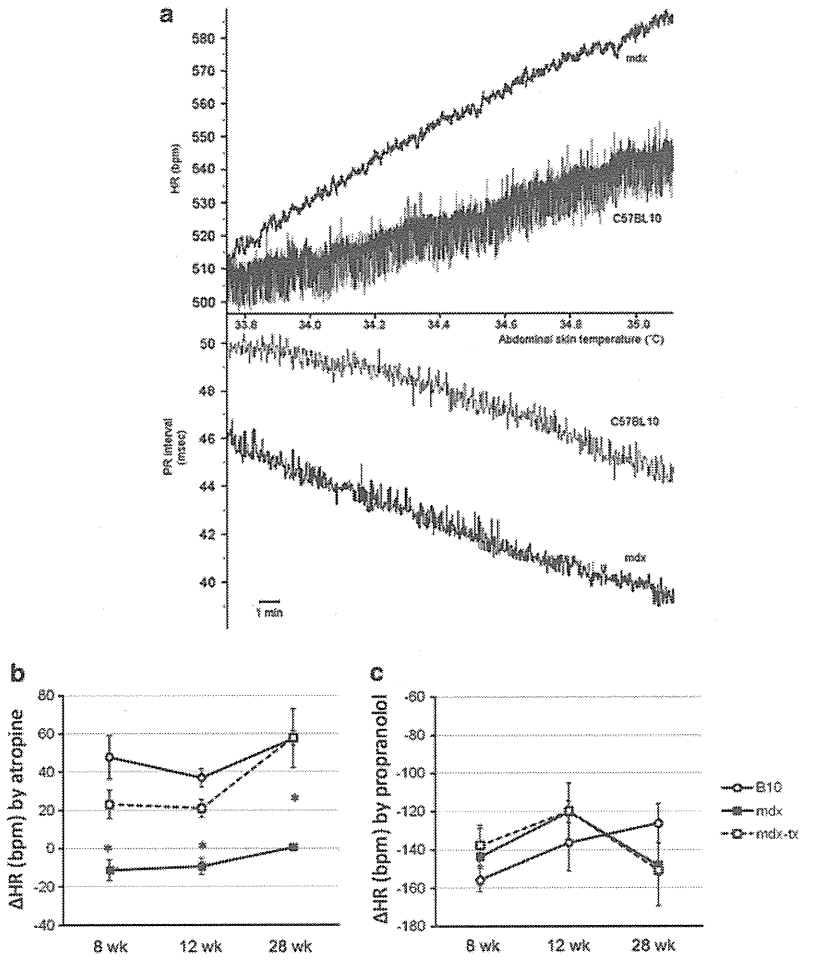

Figure 3 Dynamics of heart rate and PR intervals. (**a**) Heart rate and PR interval changes according to body temperature. Changes in heart rate (upper graph) and PR interval (lower graph) were monitored serially with increasing body temperature in C57BL10 and untransduced *mdx* mice (mdx) at the age of 12 weeks, Scale bar, 1 min. (**b**) Heart rate changes in response to atropine. The horizontal axis represents age. Data are shown as mean ± s.e.m. *$P<0.01$ between C57BL10 mice (B10) and untransduced *mdx* mice, and also between transduced *mdx* mice (mdx-tx) and untransduced *mdx* mice (n=3–4 per group at each time point). (**c**) Heart rate changes of the mice in response to propranolol (n=3–4 per group at each time point).

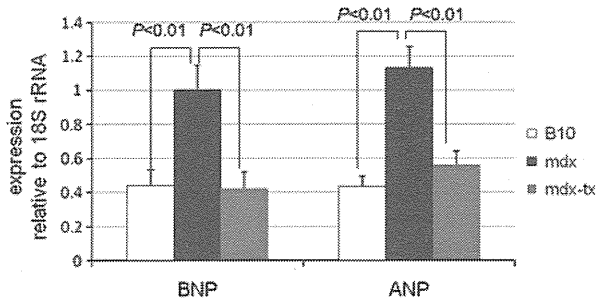

Figure 4 BNP and ANP expression in cardiac tissues. mRNA levels of BNP (**a**) and ANP (**b**) in C57BL10 (B10), untransduced *mdx* (mdx) and transduced *mdx* (mdx-tx) mice, relative to the expression of 18S rRNA. *mdx* Mice 24 weeks after transduction and control mice at the same age were evaluated. Data are shown as the mean ± s.e.m., n=3 per group.

transduction did not significantly improve running speed (data not shown, untransduced mice, 12.14 ± 8.60 m per minute; *microdystrophin* transduced mice, 23.01 ± 2.88 m per minute).

Improved survival by *microdystrophin* transduction

The cumulative survival rate of the *microdystrophin*-transduced *mdx* mice at the age of 88 weeks was 81.8% (n=11, data not shown), which was higher than that of the untransduced *mdx* mice (36.3%, n=68, $P<0.01$, Kaplan–Meier analysis).

DISCUSSION

In this study, we demonstrated effective prevention of cardiac fibrosis by transduction of *mdx* mice with *microdystrophin*. Furthermore, improvement of various ECG abnormalities as well as echocardiographic parameters was also demonstrated in the aged *mdx* mice. The transduction efficiency achieved with rAAV9 was nearly complete, with persistent expression for 74 weeks after transduction. This performance is likely due to both the strong affinity of the rAAV9 for cardiac tissue and the therapeutic effect of the expressed *microdystrophin* in preventing the degeneration of the cardiomyocytes. However, in quadriceps, the copy number of *microdystrophin* mRNA in transduced *mdx* mice was significantly lower than that of *dystrophin* in C57BL10 mice and the expression of *microdystrophin* in the skeletal muscle was <10% at 24 weeks after transduction which is below the

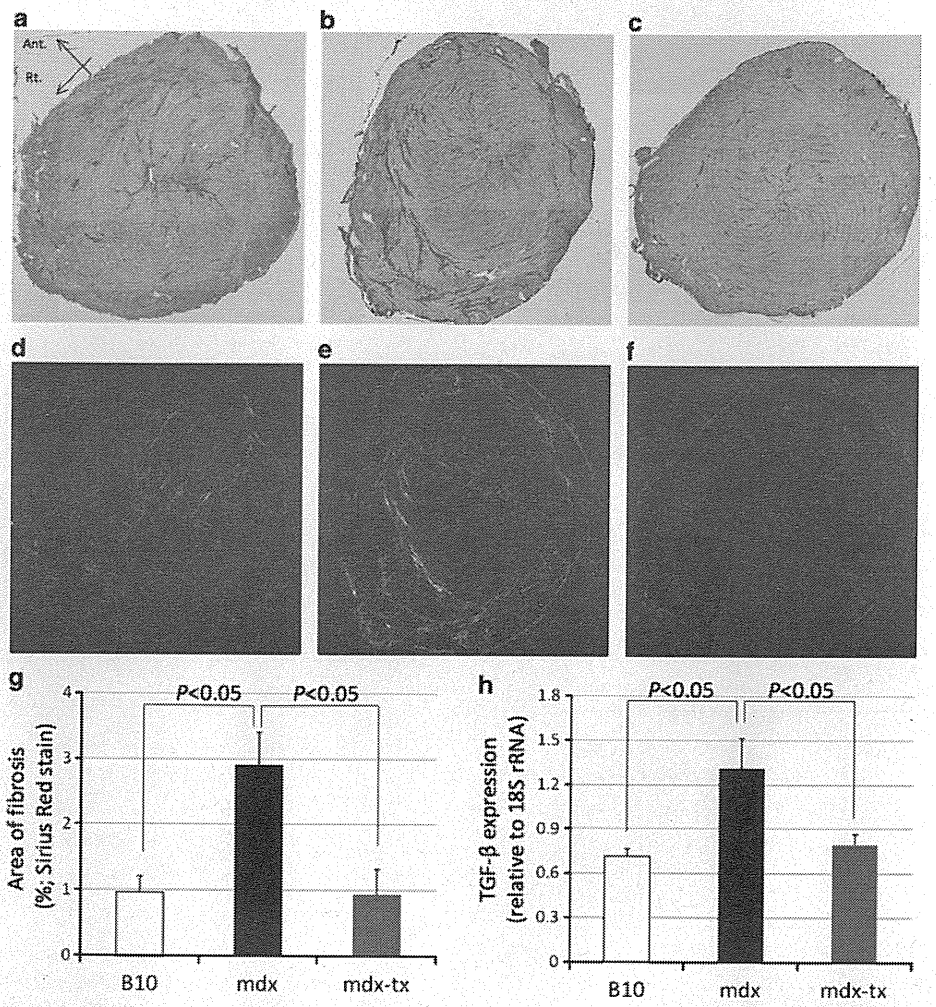

Figure 5 Fibrosis in the epimyocardium. Transverse sections of mid-ventricular level at 24 weeks after transduction. Red areas in the unpolarized views (**a–c**) and bright areas in the polarized views (**d–f**) represent fibrosis. Untransduced *mdx* mice (**b**, **e**) show extensive fibrosis in the epimyocardial area, while fibrosis is not evident in transduced *mdx* mice (**c**, **f**). (**g**) Quantification of the areas of these cardiac fibrosis, n=3 per group. (**h**) mRNA levels of TGF-β in each group, n=3 per group.

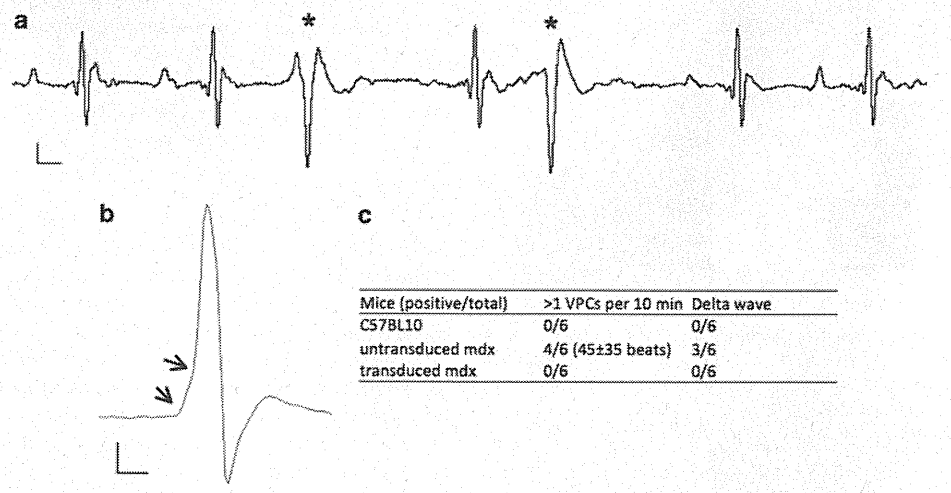

Mice (positive/total)	>1 VPCs per 10 min	Delta wave
C57BL10	0/6	0/6
untransduced mdx	4/6 (45±35 beats)	3/6
transduced mdx	0/6	0/6

Figure 6 Various ECG abnormalities in aged *mdx* mice. (**a**) Various ECG abnormalities were evident in untransduced *mdx* mice at 76 weeks of age. Representative ECG tracings show the presence of VPCs (*). Horizontal scale bar, 20 ms; vertical scale bar, 100 μV. (**b**) Pre-excitation patterns in the QRS complex. Arrows, δ wave; horizontal scale bar, 5 ms; vertical scale bar, 100 μV. (**c**) Summary of the ECG abnormalities in aged mice.

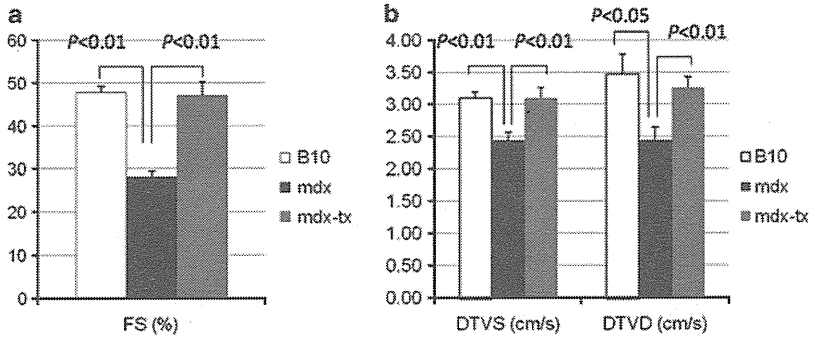

Figure 7 Echocardiograms of aged mice. (**a**) Fractional shortening (FS, %) of the left ventricle at 76 weeks of age, n=4–5 per group. (**b**) Doppler tissue velocities at 76 weeks of age, n=4–5 per group. DTVS, systolic Doppler tissue velocity; DTVD, diastolic Doppler tissue velocity. B10, C57BL10 mice; mdx, untransduced *mdx* mice; mdx-tx, *mdx* mice transduced with *microdystrophin*.

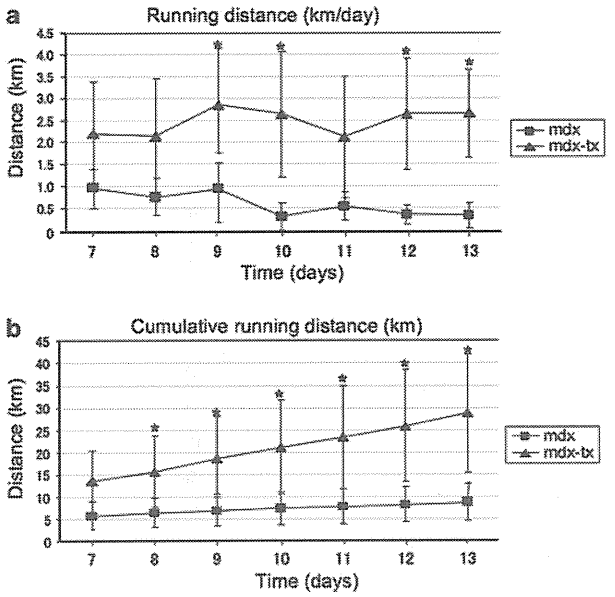

Figure 8 Voluntary wheel running. A computerized wheel system was utilized to estimate daily running distance (**a**) and cumulative running distance (**b**). Mice were housed in cages equipped with 12 cm diameter stainless steel running wheels and allowed for free access to the wheel 24 h everyday. Each wheel rotation resulted in a micro-switch closure that was recorded and stored on a computer-based data acquisition system. The running distance was recorded every 2 min. *P<0.05.

estimated therapeutic level. Therefore, at the transduction condition used in this study, the heart is supposed to be the only organ benefited by transduced *microdystrophin*. Others performed time course assay of the rAAV9-mediated transgene expression in cardiac and skeletal muscles of neonatal mice.[24] After the intravenous administration of the rAAV9, the amount of transgene expression in cardiac tissue was consistently as well as significantly higher than that in skeletal muscle and continued to steadily increase throughout the duration of the experiment. Intravenous administration of the rAAV9 into adult mice also demonstrated a marker gene expression profile similar to that found in newborns. The vector genome bio-distribution profile observed in the nonhuman primate demonstrated a dramatic preference for cardiac tissue over skeletal muscle.[24] Although theories to explain the phenomenon have currently been investigated, the preferential expression might be magnified by an increased kinetics of double-stranded DNA synthesis, annealing, uncoating and/or trafficking.

The *mdx* mice exhibited increased heart rates and shortened PR intervals compared with the background strain beginning at 8 weeks of age, which coincides with the earliest instances of cardiac dysfunction reported in *mdx* mice.[25] During this period, hemodynamic changes are not evident unless the mice are stressed,[26,27] and an increased heart rate is suggestive of compensation for compromised cardiac output. We showed that at 28 weeks of age, *mdx* mice develop heart failure that is associated with increased levels of BNP and ANP (Figure 4) as well as fibrotic infiltration (Figure 5). The autonomic nervous system has a major role in the effort to offset the effects of heart failure, primarily by influencing heart rate through the activation of the sympathetic nervous system or the inactivation of the parasympathetic nervous system.[28] However, increased sympathetic activity does not appear to be the primary cause of increased heart rate in this study. Furthermore, we observed a paradoxical heart rate drop in *mdx* mice in response to sympathetic blockade, as has been reported elsewhere.[23] In a dog model of induced heart failure, the onset of heart failure attenuates parasympathetic control of the heart and upregulates muscarinic receptor expression in the heart.[29] We believe this explains both the increase in resting heart rate in the *mdx* mice and the paradoxical response to atropine.[30]

The shortened PR interval is likely the result of a compensatory autonomic influence rather than an indication of a pre-excitation syndrome such as Lown–Ganong–Levine syndrome.[31] In this study, the shortened PR interval was clearly accompanied by sinus tachycardia and changes in the dynamic range of heart rate in response to temperature (Figure 3a). The predominant pathologic feature in the *mdx* mouse heart is dilated cardiomyopathy, rather than cardiac hypertrophy such as in Pompe[32] or Fabry disease.[33] A pre-excitation pattern in QRS complexes, which is a sign of structural AV node involvement, appeared only in older mice (Figures 6b and c).

With regard to intraventricular conduction patterns, prolongation of the QRS complex duration and reduced S/R ratio were prominent. In our series of *mdx* mice, these abnormalities became evident later than abnormalities in cardiac rhythm, but did not develop in C57BL10 or transduced *mdx* mice. Because prolongation of the QRS complex duration occurs as a manifestation of heart failure due to left ventricular dyssynchrony,[34] its prevention in the transduced *mdx* mice can be assumed to be a therapeutic effect of microdystrophin expression against the development of dilated cardiomyopathy. Reduction of the S/R ratio is another indication of intraventricular conduction abnormalities in *mdx* mice.[35] It initially appeared at ~8

weeks of age and progressively worsened (Figure 2g).[35] It is not likely to be the result of cardiac axis deviation, as it can be detected to a similar degree in any of the limb leads (Supplementary Figure 3). Therefore, changes in the S/R ratio might be due to epimyocardial distribution of cardiac fibrosis, which is evident in untransduced *mdx* mice in this study as well as in autopsy cases of DMD patients.[36] Expression of *microdystrophin* in *mdx* mice successfully repressed myocardial damage and inhibited the development of cardiac fibrosis (Figure 5) throughout the myocardium.

ECG parameters in the aged mice group were somewhat misleading, possibly confounded by decompensation of heart failure (Figure 2). In aged mice, ECG findings such as VPCs and pre-excitation patterns of the QRS complex were more indicative of the therapeutic effects of microdystrophin (Figure 6). In addition, we detected echocardiographic abnormalities in aged *mdx* mice, as has been reported previously,[26] and demonstrated prevention of cardiac dysfunction in aged mice by *microdystrophin* transduction (Figure 7).

Voluntary exercise performance was monitored on the untransduced and *microdystrophin*-transduced *mdx* mice. Compared with the untransduced *mdx* mice, daily running distances were significantly longer in the *microdystrophin*-transduced *mdx* mice. Voluntary running is an endurance exercise that reflects cardiac function. rAAV9-mediated long-term expression of *microdystrophin* might be cardioprotective and ameliorate running performance in the dystrophin-deficient *mdx* mouse with improved survival.

We demonstrated that ECG findings reveal early signs of dystrophin-deficient cardiomyopathy[5] and are helpful for monitoring the progression of cardiomyopathy in the course of gene transduction experiments. In addition, this is the first long-term study describing the therapeutic effects of *microdystrophin* transduction against dystrophin-deficient cardiomyopathy. The results presented here are promising in that microdystrophin was able to prevent both functional and pathologic deterioration until the mice reached advanced age. Considering the fact that cardiac fibrosis was prevented up to the period of advanced age, our results present the possibility that microdystrophin might be effective in the treatment of both DMD and BMD-related cardiomyopathy.

MATERIALS AND METHODS

Construction of proviral plasmid and recombinant AAV vector production

The AAV vector plasmid, pAAV *hΔCS2*, harboring a human *microdystrophin* gene *hΔCS2* expression cassette flanked by ITRs was described before.[12,37] The proviral vector plasmid pAAV *hΔCS2*, an AAV9 helper plasmid pAAV2/9 (a gift from Dr James M Wilson),[38] and an adenoviral helper plasmid pAdeno[39] were transfected into HEK293 cells at 60% confluence in a 10-tray Cell Factory (Nunc, Thermo Fisher, Roskilde Site, Denmark), and incubated for 48 h at 37 °C and 5% CO_2 with use of the active gassing technique.[40] The rAAV particles were purified by the dual ion-exchange procedures with the high-performance membrane adsorbers.[41] The viral titers were determined by quantitative PCR using the MyiQ single-color detection system (Bio-Rad, Hercules, CA, USA) with primer sets designed to specifically target the N-terminus of *hΔCS2* (forward 5′-CCAAAAGAAAAAGGATCCACAA-3′, reverse 5′-TTCCAAATCAAACCAAGAGTCA-3′).

Animal transduction

All experimental procedures were approved by the Experimental Animal Care and Use Committee at the National Institute of Neuroscience (NIN, Tokyo, Japan). *mdx* Mice and background strain C57BL10 mice were purchased from The Jackson Laboratory (Bar Harbor, ME, USA) and maintained under the standard protocol for animal care at the NIN. We performed systemic *microdystrophin* transduction in 4 weeks old *mdx* mice, so that the time of gene transduction correlated with the stage of DMD/BMD progression in patients at the time of initial diagnosis, at which point skeletal muscle pathology has already developed, but cardiomyopathy is not yet evident. Mice were injected with 3.0×10^{12} viral genomes/body via the tail vein at 4 weeks old. An equal volume of PBS was injected into mice in the control groups. The mice were killed at 24 or 74 weeks after the injection. Samples were taken from the heart, diaphragm and quadriceps and frozen in liquid nitrogen-cooled isopentane. Six to eight mice from each group were used for each time point.

Electrocardiogram

All ECGs were performed under general inhalation anesthesia with 2% isoflurane using a precision vaporizer (Shinano, Tokyo, Japan) at 4, 8, 24 and 72 weeks after transduction. Mice were placed in a closed box to minimize light and noise, and abdominal skin temperature was controlled at 35 ± 0.1 °C using an electric heating pad under the mouse in the prone position. Electrodes were placed subcutaneously on the distal limbs and readings from lead II were recorded. The PowerLab data acquisition system with Chart-Pro 6 software (AD Instruments, Bella Vista, NSW, Australia) was used for recording and analysis. ECG tracings were accepted as valid only when the values remained stabilized for 2 min. Pharmacological autonomic blockade was performed immediately after the baseline recording. Propranolol (1 mg kg^{-1} bodyweight) or atropine (0.5 mg kg^{-1} bodyweight) was injected intraperitoneally to induce sympathetic or parasympathetic blockade, respectively. Mice subjected to autonomic blockade were excluded from ECG recordings for the following 48 h. The S/R ratio represents the ratio of the amplitude of S waves to R waves on lead II.[35]

Immunofluorescence staining of dystrophin/microdystrophin

Slide mounted sections measuring 8 μm thick from the heart, diaphragm and quadriceps were stained according to the following procedure. First, the blocking solution from the Mouse-on-Mouse kit (Vector Laboratories, Burlingame, CA, USA) was applied for 1 h at room temperature. The slides were then washed with PBS and incubated with the mouse anti-dystrophin monoclonal antibody NCL-DysB (Novocastra, Newcastle, UK) at a 1:100 dilution for 1 h at room temperature, and then with Alexa Fluor 568 goat anti-mouse IgG (Invitrogen, Carlsbad, CA, USA) diluted to 1:1000. Fluorescence imaging was performed with a BZ-9000 microscope (Keyence, Osaka, Japan) using a tiling method.

Quantitative RT–PCR of dystrophin/microdystrophin, BNP, ANP and TGF-β

Total RNA was extracted from frozen mouse heart and quadriceps muscle tissue using TRIzol reagent (Invitrogen), and converted to cDNA with the QuantiTect Reverse Transcription Kit (Qiagen, Hilden, Germany). Expression levels were determined by quantitative PCR using the MyiQ single-color detection system (Bio-Rad), and normalized to the expression of 18S rRNA. Primers for each gene were designed based on the mouse genome in the NCBI Reference Sequence database[42] as follows: dystrophin/microdystrophin, forward 5′-CCAA ACAAAGTGCCCTACTATATCAA-3′, reverse 5′-GCTCAAGAGATCCAAGCAA AGG-3′; BNP, forward 5′-GGTCCAGCAGAGACCTCAAAAT-3′, reverse 5′-AG ACCCAGGCAGAGTCAGAAAC-3′; ANP, forward 5′-GATTGGAGCCCAGAG TGGACTA-3′, reverse 5′-TCGTGATAGATGAAGGCAGGAA-3′; TGF-β, forward 5′-GGAGAGCCCTGGATACCAACTA-3′, reverse 5′-CTGTGTGTCCAGG CTCCAAATA-3′; 18S rRNA, forward 5′-ACCGCAGCTAGGAATAATGGAA-3′, reverse 5′-CCTCCGACTTTCGTTCTTGATT-3′.

Western blot analysis

Samples from hearts were taken from the mid-ventricle and suspended in 100 μl of sodium dodecyl sulfate–polyacrylamide gel electrophoresis lysis buffer (10% sodium dodecyl sulfate, 70 mM Tris–HCl, 5% β-mercaptoethanol, 10 mM ethylenediaminetetraacetic acid) at 90 °C for 10 min. In all, 10 μg of protein from each sample was separated on an sodium dodecyl sulfate–polyacrylamide gel. The separated proteins were then transferred to a polyvinylidene difluoride membrane (Millipore, Billerica, MA, USA) using semi-dry transfer for 1 h. The membrane was then incubated with the following primary antibodies: NCL-DysB for dystrophin/microdystrophin, and sarcomeric α-actinin antibody EA-53 (Abcam, Cambridge, UK) for internal

control. The membrane was further washed and incubated with secondary antibody: anti-mouse IgG conjugated with HRP (Amersham Biosciences, Fairfield, CT, USA). The signals were detected using enhanced chemiluminescence (Amersham Biosciences).

Estimation of cardiac fibrosis

Sirius red staining solution was prepared by dissolving 0.5 g of Sirius red F3B (Sigma Aldrich, St Louis, MO, USA) in a saturated aqueous solution of picric acid (Sigma Aldrich). Sections taken from frozen tissues samples were stained in the Sirius red solution for 2 min and washed twice with 0.5% acetic acid solution. Images obtained by unpolarized light microscopy were used for morphologic examination, and polarized light microscopy (Eclipse E6000, Nikon, Tokyo, Japan) was used for quantification of fibrosis. For each mouse, three mid-ventricular transverse sections were analyzed with Paint.NET image processing software (dotPDN LLC, Kirkland, WA, USA). Bright areas were measured as areas of fibrosis, and these values were then divided by the total cross-sectional area to determine the degree of cardiac fibrosis.

Echocardiography

Under 2% isoflurane general inhalation anesthesia, mice were placed in the left decubitus position over an electric heating pad. A 10-MHz echocardiographic probe (EUB-6500, Hitachi, Tokyo, Japan) was gently applied to the left hemithorax, with care taken not to induce bradycardia by chest compression. Left ventricular dimensions were measured at the papillary muscle level on the parasternal long-axis angle. Doppler tissue velocities of the left ventricular posterior wall were evaluated from the parasternal short-axis angle.[43]

Voluntary wheel running

Running activity was analyzed with a computerized wheel system. Mice were housed in cages equipped with 12 cm diameter stainless steel running wheels (WW-3302, O' Hara & Co., Ltd., Tokyo, Japan) and allowed for free access to the wheel 24 h per day. Each wheel rotation resulted in a micro-switch closure that was recorded and stored on a computer-based data acquisition system. The running distance and average running speed were recorded every 2 min.

Statistical analysis

Statistical significance was determined on the basis of an unpaired two-tailed Student's *t*-test or Kaplan–Meier analysis using Statview software (Statview; SAS Institute Inc., Cary, NC, USA). A *P*-value of <0.05 was considered significant.

CONFLICT OF INTEREST

The authors declare no conflict of interest.

ACKNOWLEDGEMENTS

We thank Dr James M Wilson for providing a helper plasmid pAAV2/9. This work was supported by a Grant for Research on Nervous and Mental Disorders, by Health Science Research Grants for Research on the Human Genome and Gene Therapy, by Research on Brain Science from the Ministry of Health, Labor, and Welfare, and by Grants in Aid for Scientific Research from the Ministry of Education, Culture, Sports, Science, and Technology.

1 Emery AE. Population frequencies of inherited neuromuscular diseases–a world survey. *Neuromuscul Disord* 1991; **1**: 19–29.
2 Aartsma-Rus A, Van Deutekom JCT, Fokkema IF, Van Ommen G-JB, Den Dunnen JT. Entries in the Leiden Duchenne muscular dystrophy mutation database: an overview of mutation types and paradoxical cases that confirm the reading-frame rule. *Muscle Nerve* 2006; **34**: 135–144.
3 Bushby K, Muntoni F, Bourke JP. 107th ENMC international workshop: the management of cardiac involvement in muscular dystrophy and myotonic dystrophy. 7th–9th June 2002, Naarden, the Netherlands. *Neuromuscul Disord* 2003; **13**: 166–172.
4 Moxley RT. Clinical overview of Duchenne muscular dystrophy. In: Chamberlain J, Rando T (eds). *Duchenne Muscular Dystrophy: Advances in Therapeutics.* Taylor & Francis Group: New York, 2006, pp 1–20.
5 Nigro G, Comi LI, Politano L, Nigro G. Cardiomyopathies associated with muscular dystrophies. In: Engel A, Franzini-Armstrong C (eds). *Myology: Basic and Clinical.* McGraw-Hill: New York, 2004, pp 1239–1256.
6 Connuck DM, Sleeper LA, Colan SD, Cox GF, Towbin JA, Lowe AM *et al.* Characteristics and outcomes of cardiomyopathy in children with Duchenne or Becker muscular dystrophy: a comparative study from the Pediatric Cardiomyopathy Registry. *Am Heart J* 2008; **155**: 998–1005.
7 Gray SJ, Samulski RJ. Optimizing gene delivery vectors for the treatment of heart disease. *Expert Opin Biol Ther* 2008; **8**: 911–922.
8 Hoffman EP, Brown RH, Kunkel LM. Dystrophin: the protein product of the Duchenne muscular dystrophy locus. *Cell* 1987; **51**: 919–928.
9 Dong JY, Fan PD, Frizzell RA. Quantitative analysis of the packaging capacity of recombinant adeno-associated virus. *Hum Gene Therapy* 1996; **7**: 2101–2112.
10 Yuasa K, Miyagoe Y, Yamamoto K, Nabeshima Y, Dickson G, Takeda S. Effective restoration of dystrophin-associated proteins *in vivo* by adenovirus-mediated transfer of truncated dystrophin cDNAs. *FEBS Lett* 1998; **425**: 329–336.
11 Sakamoto M, Yuasa K, Yoshimura M, Yokota T, Ikemoto T, Suzuki M *et al.* Micro-dystrophin cDNA ameliorates dystrophic phenotypes when introduced into mdx mice as a transgene. *Biochem Biophys Res Commun* 2002; **293**: 1265–1272.
12 Yoshimura M, Sakamoto M, Ikemoto M, Mochizuki Y, Yuasa K, Miyagoe-Suzuki Y *et al.* AAV vector-mediated microdystrophin expression in a relatively small percentage of mdx myofibers improved the mdx phenotype. *Mol Ther* 2004; **10**: 821–828.
13 Gregorevic P, Allen JM, Minami E, Blankinship MJ, Haraguchi M, Meuse L *et al.* rAAV6-microdystrophin preserves muscle function and extends lifespan in severely dystrophic mice. *Nat Med* 2006; **12**: 787–789.
14 Ohshima S, Shin JH, Yuasa K, Nishiyama A, Kira J, Okada T *et al.* Transduction efficiency and immune response associated with the administration of AAV8 vector into dog skeletal muscle. *Mol Ther* 2009; **17**: 73–80.
15 Inagaki K, Fuess S, Storm TA, Gibson GA, McTiernan CF, Kay MA *et al.* Robust systemic transduction with AAV9 vectors in mice: efficient global cardiac gene transfer superior to that of AAV8. *Mol Ther* 2006; **14**: 45–53.
16 Bulfield G, Siller WG, Wight PA, Moore KJ. X chromosome-linked muscular dystrophy (mdx) in the mouse. *Proc Natl Acad Sci USA* 1984; **81**: 1189–1192.
17 Sicinski P, Geng Y, Ryder-Cook AS, Barnard EA, Darlison MG, Barnard PJ. The molecular basis of muscular dystrophy in the mdx mouse: a point mutation. *Science* 1989; **244**: 1578–1580.
18 Im WB, Phelps SF, Copen EH, Adams EG, Slightom JL, Chamberlain JS. Differential expression of dystrophin isoforms in strains of mdx mice with different mutations. *Hum Mol Genet* 1996; **5**: 1149–1153.
19 Sapp JL, Bobet J, Howlett SE. Contractile properties of myocardium are altered in dystrophin-deficient mdx mice. *J Neurol Sci* 1996; **142**: 17–24.
20 Bridges LR. The association of cardiac muscle necrosis and inflammation with the degenerative and persistent myopathy of MDX mice. *J Neurol Sci* 1986; **72**: 147–157.
21 Bostick B, Yue Y, Lai Y, Long C, Li D, Duan D. Adeno-associated virus serotype-9 microdystrophin gene therapy ameliorates electrocardiographic abnormalities in mdx mice. *Hum Gene Therapy* 2008; **19**: 851–856.
22 Townsend D, Blankinship MJ, Allen JM, Gregorevic P, Chamberlain JS, Metzger JM. Systemic administration of micro-dystrophin restores cardiac geometry and prevents dobutamine-induced cardiac pump failure. *Mol Ther* 2007; **15**: 1086–1092.
23 Chu V, Otero JM, Lopez O, Sullivan MF, Morgan JP, Amende I *et al.* Electrocardiographic findings in mdx mice: a cardiac phenotype of Duchenne muscular dystrophy. *Muscle Nerve* 2002; **26**: 513–519.
24 Pacak CA, Mah CS, Thattaliyath BD, Conlon TJ, Lewis MA, Cloutier DE *et al.* Recombinant adeno-associated virus serotype 9 leads to preferential cardiac transduction *in vivo*. *Circ Res* 2006; **99**: e3–e9.
25 Janssen PML, Hiranandani N, Mays TA, Rafael-Fortney JA. Utrophin deficiency worsens cardiac contractile dysfunction present in dystrophin-deficient mdx mice. *Am J Physiol Heart Circ Physiol* 2005; **289**: H2373–H2378.
26 Quinlan JG, Hahn HS, Wong BL, Lorenz JN, Wenisch AS, Levin LS. Evolution of the mdx mouse cardiomyopathy: physiological and morphological findings. *Neuromuscul Disord* 2004; **14**: 491–496.
27 Yue Y, Skimming JW, Liu M, Strawn T, Duan D. Full-length dystrophin expression in half of the heart cells ameliorates beta-isoproterenol-induced cardiomyopathy in mdx mice. *Hum Mol Genet* 2004; **13**: 1669–1675.
28 Mann DL. Heart failure and cor pulmonale. In: Fauci AS, Braunwald E, Kasper DL *et al.* (eds) *Harrison's Principles of Internal Medicine.* 17th edn. chapter 227. McGraw Hill: New York, 2008, pp 1443–1457.
29 Dunlap ME, Bibevski S, Rosenberry TL, Ernsberger P. Mechanisms of altered vagal control in heart failure: influence of muscarinic receptors and acetylcholinesterase activity. *Am J Physiol Heart Circ Physiol* 2003; **285**: H1632–H1640.
30 Das G, Talmers FN, Weissler AM. New observations on the effects of atropine on the sinoatrial and atrioventricular nodes in man. *Am J Cardiol* 1975; **36**: 281–285.
31 Benditt DG, Pritchett LC, Smith WM, Wallace AG, Gallagher JJ. Characteristics of atrioventricular conduction and the spectrum of arrhythmias in Lown-Ganong-Levine syndrome. *Circulation* 1978; **57**: 454–465.
32 Ansong AK, Li JS, Nozik-Grayck E, Ing R, Kravitz RM, Idriss SF *et al.* Electrocardiographic response to enzyme replacement therapy for Pompe disease. *Genet Med* 2006; **8**: 297–301.
33 Linhart A, Lubanda JC, Palecek T, Bultas J, Karetová D, Ledvinová J *et al.* Cardiac manifestations in Fabry disease. *J Inherit Metab Dis* 2001; **24**(Suppl 2): 75–83.
34 Kashani A, Barold SS. Significance of QRS complex duration in patients with heart failure. *J Am Coll Cardiol* 2005; **46**: 2183–2192.
35 Bia BL, Cassidy PJ, Young ME, Rafael JA, Leighton B, Davies KE *et al.* Decreased myocardial nNOS, increased iNOS and abnormal ECGs in mouse models of Duchenne muscular dystrophy. *J Mol Cell Cardiol* 1999; **31**: 1857–1862.

36 Frankel KA, Rosser RJ. The pathology of the heart in progressive muscular dystrophy: epimyocardial fibrosis. *Hum Pathol* 1976; **7**: 375–386.
37 Yuasa K, Sakamoto M, Miyagoe-Suzuki Y, Tanouchi A, Yamamoto H, Li J *et al.* Adeno-associated virus vector-mediated gene transfer into dystrophin-deficient skeletal muscles evokes enhanced immune response against the transgene product. *Gene Therapy* 2002; **9**: 1576–1588.
38 Lin J, Zhi Y, Mays L, Wilson JM. Vaccines based on novel adeno-associated virus vectors elicit aberrant CD8+ T-cell responses in mice. *J Virol* 2007; **81**: 11840–11849.
39 Matsushita T, Elliger S, Elliger C, Podsakoff G, Villarreal L, Kurtzman GJ *et al.* Adeno-associated virus vectors can be efficiently produced without helper virus. *Gene Therapy* 1998; **5**: 938–945.
40 Okada T, Nomoto T, Yoshioka T, Nonaka-Sarukawa M, Ito T, Ogura T *et al.* Large-scale production of recombinant viruses by use of a large culture vessel with active gassing. *Hum Gene Ther* 2005; **16**: 1212–1218.
41 Okada T, Nonaka-Sarukawa M, Uchibori R, Kinoshita K, Hayashita-Kinoh H, Nitahara-Kasahara Y *et al.* Scalable purification of adeno-associated virus serotype 1 (AAV1) and AAV8 vectors, using dual ion-exchange adsorptive membranes. *Hum Gene Ther* 2009; **20**: 1013–1021.
42 Pruitt KD, Tatusova T, Klimke W, Maglott DR. NCBI reference sequences: current status, policy and new initiatives. *Nucleic Acids Res* 2009; **37**: D32–D36.
43 Fayssoil A. Tissue Doppler characterization of cardiac phenotype in mouse. *Eur J Radiol* 2009; **72**: 82–84.

Supplementary Information accompanies the paper on Gene Therapy website (http://www.nature.com/gt)

Neuroscience 193 (2011) 249–258

LOCAL AND RETROGRADE GENE TRANSFER INTO PRIMATE NEURONAL PATHWAYS VIA ADENO-ASSOCIATED VIRUS SEROTYPE 8 AND 9

Y. MASAMIZU,[a1] T. OKADA,[b] K. KAWASAKI,[c] H. ISHIBASHI,[a] S. YUASA,[d] S. TAKEDA,[b] I. HASEGAWA[c] AND K. NAKAHARA[a]*

[a]*Department of Neurophysiology, National Institute of Neuroscience, NCNP, 4-1-1 Ogawa-Higashi, Kodaira, Tokyo 187–8502, Japan*

[b]*Department of Molecular Therapy, National Institute of Neuroscience, NCNP, 4-1-1 Ogawa-Higashi, Kodaira, Tokyo 187–8502, Japan*

[c]*Department of Physiology, Niigata University School of Medicine, 1 Asahimachi-dori, Niigata, Niigata 951-8510, Japan*

[d]*Department of Ultrastructural Research, National Institute of Neuroscience, NCNP, 4-1-1 Ogawa-Higashi, Kodaira, Tokyo 187–8502, Japan*

Abstract—Viral vector-mediated gene transfer has become increasingly valuable for primate brain research, in particular for application of genetic methods (e.g. optogenetics) to study neuronal circuit functions. Neuronal cell tropisms and infection patterns are viable options for obtaining viral vector-mediated transgene delivery that is selective for particular neuronal pathways. For example, several types of viral vectors can infect axon terminals (retrograde infections), which enables targeted transgene delivery to neurons that directly project to a particular viral injection region. Although recent studies in rodents have demonstrated that adeno-associated virus serotype 8 (AAV8) and 9 (AAV9) efficiently transduce neurons, the tropisms and infection patterns remain poorly understood in primate brains. Here, we constructed recombinant AAV8 or AAV9, which expressed an enhanced green fluorescent protein (EGFP) gene driven by a ubiquitous promoter (AAV8-EGFP and AAV9-EGFP, respectively), and stereotaxically injected it into several brain regions in marmosets and macaque monkeys. Immunohistochemical analyses revealed almost exclusive colocalization of EGFP fluorescence via AAV9-mediated gene transfer with a neuron-specific marker, indicating endogenous neuronal tropism of AAV9, which was consistent with our previous results utilizing AAV8. Injections of either AAV8-EGFP or AAV9-EGFP into the marmoset striatum resulted in EGFP expression in local striatal neurons as a result of local infection, as well as expression in dopaminergic neurons of the substantia nigra via retrograde transport along nigrostriatal axonal projections. Retrograde infections were also observed in the frontal cortex and thalamus, which are known to have direct projections to the striatum. These local and retrograde gene transfers were further demonstrated in the geniculocortical pathway of the marmoset visual system. These findings indicate promising capabilities of AAV8 and AAV9 to deliver molecular tools into a range of primate neural systems in pathway-specific manners through their neuronal tropisms and infection patterns.

Key words: AAV8, AAV9, common marmoset, gene transfer, macaque monkey, neuronal pathway.

The utilization of nonhuman primates as animal models for neuroscience research has provided a better understanding of mechanisms of high-level brain functions (Felleman and Van Essen, 1991; Nakahara et al., 2007; Passingham, 2009). Although lesion, anatomical and electrophysiological studies have revealed neural substrates and activities in primate brains, the lack of effective methods has hampered efforts to correlate detailed neural circuits with functions. Recently developed genetic methods provide promise for facilitating such studies, especially by the use of genetically encoded modulators, which have the ability to turn neuronal activity on or off with high spatiotemporal precision (Tan et al., 2006; Zhang et al., 2007; Han et al., 2009). A major hurdle for the application of genetic methods has been the specific *in vivo* expression of transgenes encoding relevant molecules in neurons of the central nervous system (CNS). In primates, although a few cases have proven successful (Chan et al., 2001; Sasaki et al., 2009), the use of generations of transgenic animals remains impractical. Therefore, gene transfer vectors could serve as a useful method for delivering transgenes into the primate CNS.

Adeno-associated viruses (AAV) are used as transgene vectors within the CNS, because they can readily infect postmitotic cells (Kaplitt et al., 1994; Kaspar et al., 2002; Hollis et al., 2008; Towne et al., 2010). Diverse AAV serotypes exist because of variations of capsid proteins, which also act as tropism determinants. Although the AAV serotype 2 (AAV2) has been most frequently used, recent attempts have sought to determine suitable AAV serotypes for target cell types, tissues, and species (Gao et al., 2002, 2004; Tan et al., 2006). Rodent studies have demonstrated that AAV8 and AAV9 are suitable for transgene deliveries into neuronal cells (Broekman et al., 2006; Taymans et al., 2007; Foust et al., 2009, 2010), and recently, we and

[1] Present address: Division of Brain Circuits, National Institute for Basic Biology, Nishigonaka 38, Myodaiji, Okazaki, Aichi 444-8585, Japan.

*Corresponding author. Tel: +81-42-346-1724; fax: +81-42-346-1754.
E-mail address: nakahara@ncnp.go.jp (K. Nakahara).

Abbreviations: AAV8, adeno-associated virus serotype 8; AAV9, adeno-associated virus serotype 9; CAG, modified chicken β-actin promoter with a cytomegalovirus immediate early enhancer; CNS, central nervous system; DA, dopamine; EGFP, enhanced green fluorescent protein; GFAP, glial fibrillary acidic protein; LGN, lateral geniculate nucleus; NeuN, neuron-specific nuclear protein; Olig2, oligodendrocyte transcription factor 2; PBS, phosphate-buffered saline; PCR, polymerase chain reaction; SNc, substantia nigra pars compacta; SNr, substantia nigra pars reticulata; TH, tyrosine hydroxylase; WPRE, woodchuck hepatitis virus post-transcriptional regulatory element.

0306-4522/11 $ - see front matter © 2011 IBRO. Published by Elsevier Ltd. All rights reserved.
doi:10.1016/j.neuroscience.2011.06.080

others showed that AAV8 exhibits strong tropism for neurons in marmoset (Masamizu et al., 2010) and macaque monkey (Dodiya et al., 2010) brains. However, AAV9, another promising neurotropic serotype, has not yet been tested on primate brains.

Several AAV serotypes can transfer genes into neurons via local and retrograde infection. Although local infections from neuronal somata and/or dendrites allow for gene transfer into neurons surrounding the virus administration sites, retrograde infections from axon terminals provide axonal transport of viral genomes. This results in transgene expression in neuronal somata of distal regions that project to the virus administration sites, which could provide strategies for transgene delivery targeted to specific neuronal pathways. For instance, AAV-mediated retrograde gene transfers have been successful in the substantia nigra and in spinal cord motoneurons (Yasuda et al., 2007; Towne et al., 2010). Exploring the infection patterns of AAV8 and AAV9 in primate brains is, therefore, a prerequisite for utilizing these serotypes in a neuronal pathway-specific manner.

The present study initially analyzed the cell tropism of AAV9 in common marmoset and macaque monkey brains. Subsequently, we explored the infection patterns of either AAV8 or AAV9 in the marmoset brain after injection into the striatum to determine the ability of retrograde infection. Moreover, the utilization of this gene transfer strategy was demonstrated by successful application of AAV8 and AAV9 to the geniculocortical pathway of the visual system.

EXPERIMENTAL PROCEDURES

Animals

Five adult, male, common marmosets (*Callithrix jacchus*) and two adult, male, macaque monkeys (*Macaca mulatta* and *Macaca fuscata*) were used for the present study (Table 1). The marmosets were 20–59 months old (230–325 g), and the macaques were 8 years old (9.2 kg) and 7 years old (6.2 kg) at the start of the experiment. All experiments were conducted in accordance with protocols approved by the ethics committee for primate research at the National Center of Neurology and Psychiatry, Japan.

Virus production

Recombinant AAV8 and AAV9 expressing enhanced green fluorescent protein (EGFP) were produced (AAV8-EGFP and AAV9-EGFP, respectively) as previously described (Okada et al., 2005, 2009). The vector plasmid (pAAV-EGFP) contained EGFP cDNA and the woodchuck hepatitis virus post-transcriptional regulatory element (WPRE), which was expressed under control of the CAG promoter, a modified chicken β-actin promoter with a cytomegalovirus immediate early enhancer. AAV8-EGFP and AAV9-EGFP viruses were produced following triple-transfection of HEK293 cells with pAAV-EGFP, an adenoviral helper plasmid pAdeno (Matsushita et al., 1998), and a chimeric helper plasmid encoding either AAV2 rep/AAV8 cap genes or AAV2 rep/AAV9 cap genes (pAAV2-8, pAAV2-9, respectively, gifts from Dr. James M. Wilson) (Gao et al., 2002, 2004), which was mediated by calcium phosphate co-precipitation with active gassing (Okada et al., 2005). At 72 h after transfection, cell suspensions were collected, centrifuged at 300×*g* for 10 min, and resuspended in 30 ml Tris-buffered saline (100 mM Tris–HCl [pH 8.0], 150 mM NaCl). AAV8-EGFP and AAV9-EGFP viruses were harvested by five-cycle freeze-thawing of the resuspended pellet. The crude viral lysate was initially concentrated by a brief two-tier CsCl gradient centrifugation for 3 h (Okada et al., 2002) and further purified by dual ion-exchange chromatography (Okada et al., 2009). Quantitative polymerase chain reaction of DNase I-treated stocks with plasmid standards determined the final number of AAV8-EGFP and AAV9-EGFP virus particles as 3.0×10^{13} and 9.27×10^{12} vector genomes (vg)/ml, respectively.

Table 1. Injection sites and viral vectors in marmosets and macaques

	Striatum		Primary visual cortex	
Animal	Right	Left	Right	Left
Marmoset A		AAV9		
Marmoset B		AAV9		
Marmoset C		AAV8		
Marmoset D			AAV9	
Marmoset E			AAV9	AAV8
Macaque A				AAV9
Macaque B			AAV8	AAV9

Virus injection

All surgical procedures and virus injections were conducted under aseptic conditions. Animals were initially i.m. anesthetized with 15–22 mg/kg of ketamine (for marmosets) or with 5 mg/kg of ketamine and 0.03 mg/kg of medetomidine (for macaques), followed by intubation and placement in a stereotaxic apparatus. Anesthesia was then maintained with inhalation of isoflurane (1.5–2.5% in oxygen). Saturation of pulse oxygen (SpO_2), heart rate, body temperature, end-tidal CO_2 ($ETCO_2$) and O_2 (ETO_2), isoflurane (ETISO), and fraction of inspired CO_2 ($FiCO_2$), O_2 (FiO_2), and isoflurane (FiISO) were continuously monitored. Following i.m. injection of the antibiotic cefovecin, a small craniotomy (2–3 mm in diameter) was made over the area of interest, and the underlying dura was slit to allow penetration of the virus-containing 10-μl Hamilton syringe connected to a 33 G (45° angle) needle. The viral solution (3 μl) was injected at a rate of 0.25 μl/min at each site. Injection sites were determined with a stereotaxic atlas of the marmoset brain (Yuasa et al., 2010) and the macaque brain (BrainMaps.org, http://brainmaps.org/), respectively. The marmoset injection sites were aimed at the striatum: 12.0 mm anterior from the interaural line, 3.0 mm lateral (L) from the midline and 6.0 mm ventral (V) from the brain surface (Eslamboli et al., 2005), as well as the primary visual cortex: 10.0 mm posterior from the interaural line, 5.0 mm L, and 2.5 mm V (Fritsches and Rosa, 1996). After each injection, the needle was maintained in place for an additional 5 min (striatum) or 15 min (primary visual cortex), and then slowly withdrawn (2 mm/min). The macaque injection sites were aimed at the primary visual cortex. After each injection, the needle was maintained in place for an additional 5 min, and then slowly withdrawn (2 mm/min).

Immunohistochemistry

Procedures were performed as previously described (Nakahira and Yuasa, 2005; Masamizu et al., 2010). At 4 weeks postinjection, animals were deeply anesthetized with a sodium pentobarbital overdose and transcardially perfused with 4% paraformaldehyde in 0.1 M phosphate-buffered saline (PBS, pH 7.4). Brains were removed from the skull and postfixed at 4 °C for 2–3 days using the same fresh fixative. The brains were embedded in 3% agar/PBS and sliced into 100-μm thick coronal sections using a Microslicer (DTK-3000, Dosaka EM, Kyoto, Japan). After 1 h of preincubation with 10% normal goat serum at 4 °C, floating sec-